Bulletin of Mathematical Biology (2010) 72: 830–868
DOI 10.1007/s11538-009-9471-1

ORIGINAL ARTICLE

A Cell-based Model of Endothelial Cell Migration, Proliferation and Maturation During Corneal Angiogenesis

Trachette Jackson, Xiaoming Zheng*

Department of Mathematics, University of Michigan, Ann Arbor, MI 48109, USA

Received: 18 August 2008 / Accepted: 15 October 2009 / Published online: 6 January 2010

Abstract The motivation of this work stems from two critical experimental observations associated with corneal angiogenesis: (1) angiogenesis will not succeed without endothelial cell proliferation, and (2) proliferation mainly occurs at the leading edge of developing sprouts (Sholley et al., Lab. Invest. 51:624–634, 1984). To discover the underlying mechanisms of these phenomena, we develop a cell-based mathematical model that integrates a mechanical model of elongation with a biochemical model of cell phenotype variation regulated by angiopoietins within a developing sprout. This model allows for a detailed study of the relative roles of endothelial cell migration, proliferation, and maturation. The model is validated by quantitatively comparing its predictions with data derived from corneal angiogenesis experiments. We conclude that cell elasticity and cell-to-cell adhesion allow only limited sprout extension in the absence of proliferation, and the maturation process combined with bioavailability of VEGF can explain the localization of proliferation to the leading edge. We also use this model to investigate the effects of X-ray irradiation, Ang-2 inhibition, and extracellular matrix anisotropy on sprout morphology and extension.

Keywords Angiogenesis · Chemotaxis · Proliferation · Migration · Maturation · Angiopoietins

1. Introduction

Angiogenesis, the growth of new capillaries from preexisting vasculature, is crucial to many physiological and pathological processes, such as tumor growth, wound healing, and certain ocular diseases. These new capillaries eventually form a complex vascular network that penetrates the tumor or tissue and provides direct nutrient supply. During angiogenesis, tissue or tumor cells are trigged by environmental stimuli, such as injury or hypoxia, to release a wide variety of polypeptide angiogenic factors, such as vascular endothelial growth factor (VEGF). When the endothelial cells (ECs) that line the inside surfaces of blood vessels become activated by VEGF, they initiate an entire cascade of cellular events. Specifically, the stimulation of ECs by VEGF leads to the degradation of the

*Corresponding author.
E-mail addresses: tjacks@umich.edu (Trachette Jackson), xmzheng@umich.edu (Xiaoming Zheng).

basement membrane, and the directed migration of these cells, guided by a chemotactic response to VEGF, through the extracellular matrix (ECM). Neovascularization is clearly the result of many complex processes that culminate in the proliferation and migration of ECs, via their interaction with the ECM, sprout lumen formation, and the maturation of newly formed sprouts.

There are two critical experimental observations from the original work of Sholley et al. (1984) on rat corneal angiogenesis. First, without proliferation, only a restricted sprout network that never reaches the source of chemoattractant, is formed. Second, proliferation mainly occurs at the leading edge of developing sprouts. Although the processes associated with angiogenesis are the subject of many mathematical and computational investigations, none of the current mathematical approaches, including continuous models (Balding and McElwain, 1985; Byrne and Chaplain, 1995, 1996; Anderson and Chaplain, 1998a, 1998b; Levine et al., 2001a; Sleeman and Wallis, 2002; Plank and Sleeman, 2003, 2004; Plank et al., 2004; Levine and Nilsen-Hamilton, 2006), discrete models (Anderson and Chaplain, 1998b; Plank and Sleeman, 2003, 2004; Stokes and Lauffenburger, 1991; Tong and Yuan, 2001; Sun et al., 2005; Gevertz and Torquato, 2006; Milde et al., 2008), and cell-based models (Peirce et al., 2004; Bauer et al., 2007; Qutub and Popel, 2009), correctly capture the mechanisms underlying these two experimental observations. A detailed review of most of this representative, rather than comprehensive, list of models and their limitations is provided in Mantzaris et al. (2004). Interestingly, understanding the critical importance of proliferation and where it occurs during tumor angiogenesis are among the ten challenges identified therein. Carefully designed mathematical models can shed light on the interplay between different factors controlling these processes, and this is the exact focus of our work.

The key to resolving these issues is to derive correct relationships between cell proliferation, sprout extension, and sprout maturation based on experiments. To this end, the cornea is very attractive due to the accessibility and high tissue visibility of the in vivo environment. The corneal angiogenesis system is one of the most experimentally studied models of blood vessel growth, and as a result, it is also the basis and playground of many mathematical models, including (Balding and McElwain, 1985; Anderson and Chaplain, 1998a, 1998b; Levine et al., 2001a; Stokes and Lauffenburger, 1991; Harrington et al., 2007; Tong and Yuan, 2008; Addison-Smith et al., 2008). In our work, we take three main ingredients from experiments, especially from corneal angiogenesis. First, Ausprunk and Folkman (1977) and Semino et al. (2006) showed that migration is the primary event of sprout extension, and Gerhardt et al. (2003) revealed the important role of the tip cells in sprout extension. This stimulates us to study the cytoskeletal mechanics of tip cells to elucidate the sprout extension mechanism. Second, the experiments of Sholley and his collaborators (Sholley et al., 1983a, 1983b, 1984; Sholley and Wilson, 1987) are of special value for their deep insight into the relationship between migration and proliferation, and are our motivation for considering different phenotypes of cells in a capillary sprout. Third, discoveries concerning the maturation process and associated regulator angiopoietins, especially from Yancopoulos and his colleagues (Suri et al., 1996; Davis et al., 1996; Maisonpierre et al., 1997; Ashara et al., 1998), and Augustin and his colleagues (Fiedler et al., 2004; Scharpfenecker et al., 2005; Fiedler et al., 2006), make it possible to interpret the variation of proliferative activities in a developing sprout.

Based on all of these experimental findings and existing mathematical models, we develop a cell-based model that incorporates the proliferation, migration, and maturation mechanisms in combination with distinct cellular phenotypes. We use discrete points to represent each cell in a developing sprout. For the tip cell, we develop a viscoelastic equation describing its elongation, and on each stalk cell we assign continuous differential equations to model their proliferation and maturation. Throughout the tissue, we use differential equations to model the reactions and diffusion of multiple angiogenic factors. Therefore, our model includes not only cell-based discrete representations for cells, but also continuum approximations of their processes. Our model construction and the integration of previous methods is itself novel in that it is able to provide insight into the relative importance of proliferation, migration, and maturation that have not been attained with any of the previously published mathematical approaches. Many other new and important features in our model include the derivation of the force balance equation for tip ECs from general viscoelastic equations; the spring network model of the vasculature; the contribution of proliferation to sprout extension; and the model mechanism for nonproliferative sprout extension.

In this paper, we will first discuss the previous mathematical models of angiogenesis in Section 2, then introduce the basic ideas of our model in Section 3. We elaborate on the details of our model in Sections 4 to 7, including the mechanism of tip cell elongation, maturation (the quiescent transition) and proliferation of sprout cells, migration of preexisting vessel cells, and how these mechanisms are integrated to form a complete model. In Section 8, we use our model to simulate the rat corneal angiogenesis and compare the results with experimental data.

2. Review: the need for new modeling approaches

In this section, we will review some of the most representative mathematical models of angiogenesis, and try to explain why they are unable to capture several specific experimental observations. Much of the literature up to 2004 was reviewed in Mantzaris et al. (2004), however, we want to provide further insight into previous models according to the clearer picture of angiogenic processes that has emerged.

In this paper, the EC density is denoted by e, and the VEGF concentration by c.

2.1. Continuous models: single phenotype of ECs

It was common early in angiogenesis modeling to either consider only one type of EC (e.g., tip cells) or to assume that all ECs are phenotypically indistinguishable. For example, in Anderson and Chaplain (1998b), only the behavior and motion of the sprout tip cells were explicitly modeled, and the cells behind the tip were assumed to follow the path set forth by the tip cells. A typical continuous model of the sprout tip is the diffusion-advection equation:

$$\frac{\partial e}{\partial t} = D_e \nabla^2 e - \nabla \cdot \big(\chi(c) e \nabla c\big). \tag{1}$$

In (1), the chemotactic sensitivity of ECs to VEGF is represented by $\chi(c)$. Several choices of $\chi(c)$ have appeared in the literature over the years, including:

$$\chi(c) = \chi_0, \qquad \chi(c) = \frac{k_c c_g}{(c + c_g)^2}, \tag{2}$$

which are the constant law and the receptor law, respectively Chaplain (1996). The parameters χ_0, k_c, c_g are all constants, and more choices of $\chi(c)$ can be found in Othmer and Stevens (1997).

Parameters are usually chosen based on available data, so that the diffusion constant D_e is far less than the chemotactic sensitivity; therefore, Eq. (1) is advection-dominated. The geometry of most models of tumor angiogenesis is such that ∇c directs ECs toward the tumor. A common feature of the chemotactic functions listed above is that they are never zero for any finite value of c, which implies the speed of the cells is always nonzero when a nonzero gradient of the chemoattractant is present. Therefore, this type of model predicts that cells always will eventually reach the tumor, even in the absence of proliferation. One may recall that in both Anderson and Chaplain (1998a, 1998b), proliferation is not considered, yet a steady state of EC density is achieved before cells reach the tumor. However, these models are based on a special fibronectin profile that lures the EC backward while the gradient of VEGF pulls them forward. Therefore, a steady state is reached when these two forces are balanced. The dependence on such a special fibronectin configuration is likely unrealistic for complicated in vivo biological environments.

In reality, sprout extension is crucially dependent upon having a source of ECs, either from proliferation of cells in the developing vessel or from the continual recruitment of cells from the parent vessel (Sholley et al., 1984; Paweletz and Knierim, 1989; Kearney et al., 2004). So it seems that in the models of Anderson and Chaplain (1998a, 1998b), a supply of ECs by proliferation or recruitment is assumed by default, even though it was not explicitly modeled.

One approach to recover the proliferation effect is to model all the cells in the vessel and add proliferation terms as in Levine et al. (2001a):

$$\frac{\partial e}{\partial t} = D_e \nabla^2 e - \nabla \cdot \big(\chi(c) e \nabla c\big) + \beta_s e H(c - c_0) \frac{c}{c + \alpha} - \mu_s e. \tag{3}$$

Unfortunately, this model has the same problem as that of Eq. (1) because proliferation and migration are still completely separated; each cell migrates with velocity $-D_e \nabla e + \chi(c) \nabla c$ and proliferates with a rate of change of mass $\beta_s e H(c - c_0) \frac{c}{c+\alpha} - \mu_s e$. Therefore, vessels continually extend independently of proliferation.

The main difficulty with these models is a direct result of the limitations associated with the assumption of a single type of endothelial cells. In fact, the ECs in a vessel have different phenotypes, and consequently play different roles in vessel formation and extension. Therefore, it is necessary to model multiple types of ECs.

2.2. *Continuous models: multiple types of ECs*

Balding and McElwain (1985) developed the first model to incorporate multiple phenotypes, where they divided the whole vessel into two different functional parts: tips and

capillary sprouts. Later, this model was further developed by Byrne and Chaplain (1995, 1996), Pettet et al. (1996a, 1996b), Schugart et al. (2008). In such models, the tip cells can proliferate, migrate, fuse, and branch, while the capillary sprouts are "dragged" by the tips. If we denote the number density of tips and capillary sprouts as n and b, respectively, then the typical equation for the tips would be

$$\frac{\partial n}{\partial t} = -\nabla \cdot (J_n) + (\lambda_1 cb + \lambda_2 cn) - (\lambda_3 b + \lambda_4 n)n, \tag{4}$$

where the flux $J_n = -D_n \nabla n + \chi(c) n \nabla c$ as described in Eq. (1), $(\lambda_1 cb + \lambda_2 cn)$ describes the production of new tips from sprouts and tips, and $(\lambda_3 b + \lambda_4 n)n$ describes the loss of tips by sprout-tip and tip-tip anastomoses. Notice that in Eq. (4) the production of new tips is a function of VEGF.

As for the growth of capillary sprouts induced by the tip's migration, two different modeling methods are used in the literature. The first method treats it in a "snail trail" manner (e.g., Balding and McElwain, 1985; Byrne and Chaplain, 1995, 1996; Pettet et al., 1996a, 1996b), which assumes that sprouts increase at the same rate as the norm of the flux of tips, $\|J_n\|$. The addition of a diffusion term and a logistic proliferation term gives the equation for capillary sprouts density b as

$$\frac{\partial b}{\partial t} = \|J_n\| + D_b \nabla^2 b + \lambda_5 b(b_0 - b). \tag{5}$$

Another approach is to assume that sprouts are advected with the same velocity of the tips, $\frac{J_n}{n}$, and then the equation becomes

$$\frac{\partial b}{\partial t} = -\nabla \cdot \left(b g_b(n) \frac{J_n}{n} \right) + D_b \nabla^2 b + \lambda_5 b(b_0 - b), \tag{6}$$

where $g_b(n)$ is a function indicating the existence of the tips, and can be chosen as the Heaviside function of n or An/n_0 as in Schugart et al. (2008). Although these types of models make progress toward incorporating functional differences in the ECs that make up a developing sprout, they still have the same problem as models using Eq. (1), because the sprouts can still advance regardless of whether or not there is proliferation (see Eq. (4)). Another big disadvantage of such models is that they are based on the number densities of tips and sprouts. Thus, it is almost impossible to convert them to discrete models that simulate more realistic capillary structure.

In Levine and Nilsen-Hamilton (2006), ECs are divided into two phenotypes: inactive cells in G_0 phase, and active cells in phases G1, S, G2, and M. Inactive and active cells have different proliferation and migration abilities, and the transfer between these two types of cells is modeled. Although angiopoietins are not considered as mediators of phenotypic changes, this model is an important step toward the incorporation of multiple types of ECs in developing sprouts.

In Plank et al. (2004), ECs are divided into immature and mature cells, where immature cells proliferate and migrate according to Eq. (3), and mature cells basically remain proliferatively quiescent and stationary in order to form the stable stalk of the vessel. This is the first mathematical model to consider angiopoietins and their roles in vascular maturity. According to Eq. (3), immature cells will move away from mature cells and vessel

integrity will be lost. To counteract this effect, the transition from immature to mature cells is added. Without proliferation, all immature cells will convert to mature cells in finite time and then the sprouts stop growing. Therefore, this model predicts the correct vessel growth scenario in the absence of proliferation. However, there are conceptual issues with this modeling choice. Vessel integrity should be maintained by the continuous deposition of ECs into the vessel, not necessarily by waiting until immature cells reach full maturity.

2.3. Discrete models and cell-based models

Discrete models are very powerful in providing straightforward images of vessel formation. Many discrete models, including those that are discretizations of their continuous counterparts, only consider the tip cell and the vessel itself is assumed to simply follow the path of the tip cell (Anderson and Chaplain, 1998b; Plank and Sleeman, 2003, 2004; Tong and Yuan, 2001; Sun et al., 2005; Gevertz and Torquato, 2006; Milde et al., 2008). In such models, if proliferation is considered, it occurs only at the tip. However, as shown in Bauer et al. (2007), this is not adequate to achieve the correct relationship between the cell proliferation rate and the vessel extension speed. One resolution to this problem is to use a cell-based approach that can model each cell in the vessel individually. Popular cell-based approaches include cellular automata (Peirce et al., 2004), the biomechanically-based, cellular Potts approach (Bauer et al., 2007), and agent-based models (Qutub and Popel, 2009).

The stochastic model of Stokes and Lauffenburger (1991) is one of the most successful discrete models, where the motion of the tip cell is described by a stochastic differential equation. All the stalk cells in a vessel are represented by a single variable that is the averaged density along the vessel. This density changes due to proliferation, vessel extension, and cell redistribution from parent vessel to sprouts, or from one sprout to another by branching and anastomosis. If a sprout's density drops to a specified minimum value, then the velocity of the tip is set to zero, thus the vessel cannot elongate. Certain aspects of this model, such as incorporating the cell density along the vessel, provide a very good basis for future improvement, and our work is one step in this direction.

In the cell-based models mentioned above, all cells in a vessel have a finite volume in space; therefore, these approaches provide a very powerful framework for incorporating cellular dynamics and interactions between cells. In the cellular automata model of Peirce et al. (2004), the interaction between ECs, smooth muscle cells, and perivascular cells is modeled in a vessel network assembly in response to VEGF. In the cellular Potts model of Bauer et al. (2007), the interaction between ECs and ECM is simulated and the roles of migration and proliferation are carefully investigated. This model shows that if proliferation only occurs near the tip cells, and the cell turnover rate measured from experiments is used, then the vessels extend significantly more slowly than experimentally observed. The agent-based model of Qutub and Popel (2009) uses logical rules to guide the behavior of individual endothelial cells and segments of cells, and studies the effects of cell elongation, migration, and proliferation on capillary growth at the initial stage of angiogenesis. However, existing cell-based models have paid little attention to cell elasticity and cell recruitment from the parent vessel, which are known to play an important role in cell elongation (Munevar et al., 2001) and sprout extension (Sholley et al., 1984), respectively. Both of these critical components will be included in our model.

3. New model: introduction and basic assumptions

The key to modeling the angiogenesis process is to understand the relationships between extension, proliferation, and phenotypic changes of the ECs that constitute developing vessels.

3.1. Relationship between migration, proliferation, and maturation

Both proliferation and migration are important for the extension of capillary sprouts, but how these two events are coordinated during the extension process is still heavily debated. Our basic assumption is that migration is the primary event of and plays a leading role in capillary extension, while proliferation is secondary but provides the necessary material resources for capillary extension. This assumption was first proposed in Ausprunk and Folkman (1977) based on rabbit corneal experiments, and was confirmed in a series of work in Sholley et al. (1983a, 1983b, 1984), Sholley and Wilson (1987) on rat corneas, and in Semino et al. (2006) in monolayer experiments. Based on the effects of X-ray irradiation during angiogenesis on rat corneas, Sholley and his coworkers propose in Sholley et al. (1983b) that "neovascularization proceeds via two mechanisms: an initial radioresistant, nonproliferative process involving the migration and expansion of preexisting limbal ECs followed by comparatively radiosensitive proliferative growth." The analysis in Sholley et al. (1983b) shows that radioresistant, nonproliferative growth did not continue after 4 days. After that, proliferative growth dominates until the sprouts reach the angiogenesis stimulus.

Another possible source for the vessel extension is the putative endothelial progenitor cells that could mobilize from bone marrow to participate in neovascularization, which has been enthusiastically studied in recent years. However, we believe it is unlikely that the circulating ECs significantly contribute to corneal angiogenesis. In their study, Sholley et al. (1984) point out that if circulating stalk cells were an important source of new EC, then vascular extension should have continued after 4 days despite irradiation. Also, because only local irradiation was used, the bone marrow as a source of circulating EC precursors would not have been affected. Recently, experiments in Purhonen et al. (2008) show that no bone marrow-derived VEGFR-2 or other EC precursors contribute to vascular endothelium. Therefore, we will not consider the contribution of circulating ECs to angiogenesis in this work.

A common assumption in mathematical models of angiogenesis is that EC division mainly happens at the leading edge of the developing sprout, as observed in Ausprunk and Folkman (1977), Chan-Ling (1997). However, proliferation can and does happen anywhere in the stalk except at the tip cell, as seen in Gerhardt et al. (2003). In our work, we will focus on angiogenesis induced by cauterization of rat cornea. The experiments of Sholley et al. (1984) showed that 7 days post-cauterization, 66.5% of all cells undergoing DNA synthesis were located within 25% of the length of the leading edge of the vasculature. Even though most of the proliferative activity is localized to the leading edge, proliferation in other regions of the sprout is not negligible. Therefore, in our model, we will consider proliferation along the entire developing sprout.

In developing vessels, ECs depend on VEGF for survival (Benjamin et al., 1999), and later recruit pericytes to form a stabilizing and protective coating (Griffioen and Molema, 2000). This stabilization process is regulated by another important family of angiogenic

proteins, angiopoietins (Ang). Both Ang-1 (Davis et al., 1996) and Ang-2 (Maisonpierre et al., 1997) are ligands for the EC-specific tyrosine kinase receptor Tie-2. It is believed that Ang-1 is an activator of Tie-2, while Ang-2 is known to antagonize the binding of Ang-1 to Tie-2 (Augustin et al., 2009). It is established that Ang-1 enhances the interaction between ECs and pericytes and other support cells (Witzenbichler et al., 1998; Scharpfenecker et al., 2005), and the tight contact between ECs and support cells inhibits EC proliferation (Ashara et al., 1998). Therefore, Ang-1 can repress EC proliferation and render them quiescent. In contrast, Ang-2 destabilizes vessels by loosening the EC/pericyte contacts. Acting in concert with VEGF, Ang-2 may initiate and stimulate angiogenesis (Maisonpierre et al., 1997; Beck et al., 2000). However, in the absence of VEGF, Ang-2 induces vessel regression (Holash et al., 1999; Beck et al., 2000). The maturation mechanism has been confirmed in the rat corneal neovascularization experiments in Wakui et al. (2006), where pericytes were observed to surround some ECs 7 days after the onset of angiogenesis. In human corneal angiogenesis experiments (Cursiefen et al., 2003), 2 weeks after the onset of angiogenesis, more than 80% of new vessels were covered by pericytes. There are very few mathematical models of angiopoietins in angiogenesis; those that do exist include Plank et al. (2004), Gevertz and Torquato (2006), and Arakelyan et al. (2002), and to the best of our knowledge, Plank et al. (2004) and Arakelyan et al. (2002) are the only two that address the relationship between maturation and angiopoietins. The main reason behind the paucity of angiopoietin-dependent models is the lack of experimental data concerning the associated signaling pathways.

Notice that the maturation (or maturity) and the transition to quiescence (or quiescent level) are different but closely-related concepts. Maturation and the transition to quiescence are processes that cells undergo, while levels of maturity and quiescence are states that cells achieve. In general, maturation is a process characterized by the pericyte coating and stable structure. Since pericyte coating prohibits proliferation, mature cells are quiescent. Therefore, maturation implies a transition to quiescence, and full maturity implies maximum quiescent level. However, quiescence does not necessarily indicate maturity, as is the case of irradiated cells without pericyte coating. A more rigorous definition of maturity is provided in Section 6.1.

3.2. Hybrid cell-based model

The recognition of different phenotypes of ECs in a developing sprout is an exciting breakthrough in angiogenesis (Horowitz and Simons, 2008; Smet et al., 2009). More specifically, according to Gerhardt et al. (2003), the sprout tip is typically a single cell that migrates and leads the extension of the developing sprout; the tip cell generally does not proliferate, but the stalk cells are often busy with proliferation. Therefore, in our model, each sprout is divided into two parts: a single tip cell and stalk cells. A viscoelastic model of the tip cell will be discussed in Section 4. Each stalk cell proliferates, and once its mass has doubled, divides into two equal-mass daughter cells, which redistribute in space. Tip cells, as discussed in Section 7.2, dominate the motion of stalk cells. In contrast to many cell-based approaches (Peirce et al., 2004; Bauer et al., 2007; Qutub and Popel, 2009), we use discrete spatial points to track all of the cells and each point represents the front of a cell. Therefore, a sprout is represented as an array of discrete points, and the length of a cell is the distance between the discrete points representing itself and the cell behind it. On each discrete point (one cell) of the stalk, a time-continuous mass density and local maturity function are assigned.

In contrast to the use of logical rules in the above-mentioned cell-based models, we use continuous differential equations to govern cell elongation, proliferation, and maturation, and the reaction and diffusion of VEGF and the angiopoietins. Therefore, our model combines cell-based discrete representations for cells, with continuum approximations of their processes.

3.3. Setup of the corneal angiogenesis problem

In corneal angiogenesis experiments (Sholley et al., 1984; Thompson et al., 2003), silver nitrate was used to cauterize the center of the cornea and create a lesion; neovascularization was observed to occur from the limbus toward the central lesion, as illustrated in Fig. 1. Let R be the radius of the cornea bounded by the limbus, and L be the distance from limbus to the lesion edge. In this work, the entire computational domain Ω is the square $[-2.5, 2.5]^2$ mm^2 instead of the cornea disc only to simplify the generation of meshes and the finite difference schemes used in this work. The lesion Ω_T is a disc centered at $(0, 0)$ with radius $r = 0.5$ mm, and the region inside Ω excluding Ω_T is denoted as Ω_C, i.e., $\Omega_C = \Omega \backslash \Omega_T$.

As demonstrated in Amano et al. (1998), VEGF is required for rat corneal angiogenesis, and it is produced at high levels after corneal injury. Therefore, we assume VEGF is released from the lesion, diffuses with natural decay in the cornea, and is uptaken by ECs. The equation for VEGF is

$$\frac{\partial c}{\partial t} = D_c \nabla^2 c - \mu_c c - \frac{k_{\max} c e}{k_n + c}, \quad \text{in } \Omega_C, \tag{7}$$

where D_c is the diffusion constant, μ_c is the natural decay rate, $k_{\max}$ is the maximum uptake rate, k_n is the half saturation constant, and e is the EC density. The uptake term is derived based on monomeric, quasi-steady state binding of VEGF to its EC surface

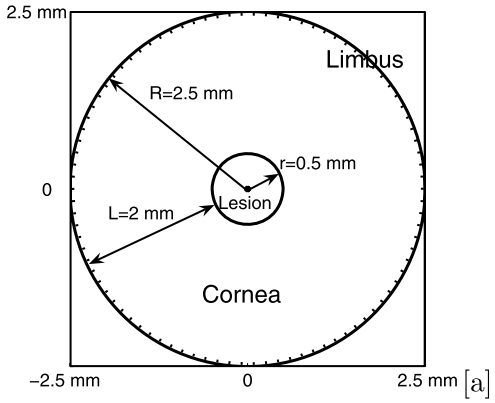

Fig. 1 The computational domain $\Omega = [-2.5, 2.5]^2$ mm^2, and the lesion Ω_T is the center disc with radius $r = 0.5$ mm. The characteristic length $L = 2$ mm is the distance between the lesion boundary and limbus. New sprouts will grow from the limbus toward the lesion.

receptor, VEGFR-2 (Jain et al., 2008). The boundary conditions are

$$c|_{\partial\Omega_T} = c_0, \qquad \left.\frac{\partial c}{\partial n}\right|_{\partial\Omega} = 0. \tag{8}$$

Inside the lesion Ω_T, we assume the value of VEGF to be c_0.

4. Tip cell elongation

In order to model migration, we must investigate the cellular level mechanics of cell motion, a schematic of which is shown in Fig. 2.

ECs send out filopodia to detect spatial differences in the concentration of VEGF, then polarize and migrate. As studied in Munevar et al. (2001), the leading edge of a cell extends lamellipodia, providing almost all of the force necessary for forward locomotion. In this work, we assume the protrusion is solely due to chemotaxis, i.e., the response to the gradient of VEGF. Therefore, the protrusion force is identical to the chemotactic force. The cell processes the chemotaxis signal, then generates the protrusion force by assembly and disassembly of actin filaments (Pollard and Borisy, 2003). Lamellipodia protrude and adhere to the ECM by focal adhesions, and pull stress fibers within the cells that contract the cell body and induce the release of the rear adhesions to the ECM, thus moving the entire cell. Notice that the generation of the protrusion force requires the firm adhesion with ECM (Lamalice et al., 2007), but this is not modeled in the current work.

In a developing sprout, however, strong cellular adhesion exists between neighboring cells, so motile cells cannot simply retract their rears. In a sprout, the chemotactic force is typically generated by the tip cell, as it likely has more freedom to extend protrusions into the ECM that sense gradients of chemoattractants (Gerhardt et al., 2003). Therefore, we assume that it is only the tip cell that generates the protrusion force in a sprout and other cells do not respond directly to chemotaxis. Furthermore, the protrusion force of the tip cell is assumed to be transduced to the whole sprout through the junctions between cells so that every cell is pulled, and the sprout stops extending when the protrusion force and the adhesion force are balanced. This balance is broken whenever a new cell is born, which acts as an unstretched spring and will be pulled in the tip direction. This allows the

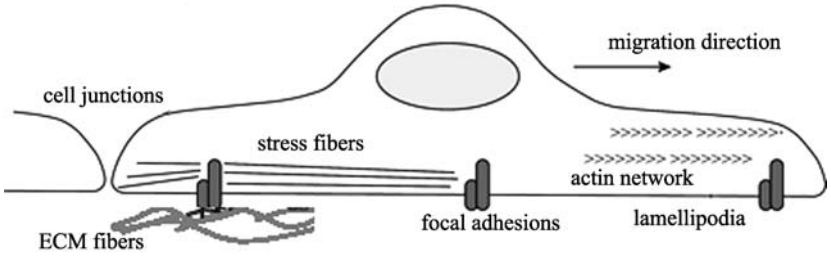

Fig. 2 Mechanics of tip cell motion. The F-actin network in lamellipodia generates a protrusion force based on focal adhesions to the ECM, which is transduced via stress fibers to the entire cell body. In order to contract its rear, the cell has to release the rear focal adhesions to ECM and overcome or disrupt adhesions with neighboring cells. Reproduced from Lamalice et al. (2007) with permission.

retraction of the tip cell so that it can migrate again. The repetition of this process extends the sprout in the chemoattractant direction.

4.1. The Spring model in one dimensional space

The tip EC can be regarded as a spring-dashpot system (Larripa and Mogilner, 2006; Gracheva and Othmer, 2004) with Young's modulus E, viscosity μ, and friction β between EC and ECM. Lamellipodia generate a protrusion force F, so that the elongation of the cell body u satisfies the force balance equation

$$\frac{EA_0}{L_0}u + \frac{\mu A_0}{L_0}\frac{du}{dt} + \beta A_1 \frac{du}{dt} = F, \tag{9}$$

where A_0 is the cross-section area, L_0 is the initial length, and A_1 is the contact area of lamellipodia with ECM. The first term is the elastic force of the spring followed by the internal viscous force. The third term is the friction or drag on the contact surface with the ECM, and the last term F is the chemotactic force. This equation has a unit of picoNewton (pN) and can be rigorously derived from the viscoelastic model with small deformation (for details, see the Appendix). To simplify the ECM dynamics, we assume the ECM will not be deformed by cells.

If all parameters and the chemotactic force F are constants, then the solution of Eq. (9) with the initial condition $u(0) = 0$ is

$$u = \frac{FL_0}{EA_0}\left(1 - e^{-t/T_0}\right), \tag{10}$$

where

$$T_0 = \frac{\mu}{E} + \frac{\beta A_1 L_0}{EA_0}. \tag{11}$$

T_0 is the typical relaxation time, and the steady state (or resting) length of the cell is $\frac{FL_0}{EA_0}$. An increase in the magnitude of chemotactic force F will result in greater elongation of the cell, which is supported by the experiments in Gerhardt et al. (2003).

The Young's modulus for ECs varies from $1.5 \times 10^3 \ \frac{\text{pN}}{\mu\text{m}^2}$ to $5.6 \times 10^3 \ \frac{\text{pN}}{\mu\text{m}^2}$ (Costa et al., 2006), and we choose an intermediate value, $2 \times 10^3 \ \frac{\text{pN}}{\mu\text{m}^2}$, from this range. The viscosity μ is not available for ECs, so we replace it with the value for fibroblasts (Thoumine and Ott, 1997): $\mu = 10^4 \ \frac{\text{pN·s}}{\mu\text{m}^2}$. The estimate of β will be highly dependent on the material, and we use the value $\beta = 1000 \ \frac{\text{pN·s}}{\mu\text{m}^3}$ from Larripa and Mogilner (2006). The protrusion force per area is about $10^4 \ \frac{\text{pN}}{\mu\text{m}^2}$ measured by Prass et al. (2006), and lamellipodia form a thin layer with height 0.2 μm and width 10 μm, thus total protrusion force F is 2×10^4 pN. An unstretched EC is roughly 10 μm long, 10 μm wide, and 1 μm thick (Levine et al., 2001a), thus $L_0 = 10$ μm and $A_0 = 10\ \mu\text{m}^2$. The length of lamellipodia L_1 is assumed to be 10 μm, so its area $A_1 = 100\ \mu\text{m}^2$. With these values, the relaxation time is $T_0 = 50$ s, and the steady state is $u = 10$ μm, and the total length of EC is $L_0 + u + L_1 = 30$ μm, which is a reasonable estimate (Gerhardt et al., 2003).

For the protrusion force F, if we assume the receptor law (e.g., Othmer and Stevens, 1997), then

$$F = k_c \frac{\alpha_1}{(c+\alpha_1)^2} \nabla c. \tag{12}$$

This form predicts that if ∇c goes to infinity while c remains bounded, the force will blow up, which should not be the case because the actin filaments available for ECs to generate forces are limited. Thus, an upper bound for the force should exist, so we choose an upper bound $\frac{|\nabla c|+\alpha_2}{|\nabla c|+\alpha_3} \frac{\nabla c}{|\nabla c|}$ in the direction of ∇c and modify the force to be

$$F = k_d \frac{\alpha_1}{(c+\alpha_1)^2} \frac{|\nabla c|+\alpha_2}{|\nabla c|+\alpha_3} \frac{\nabla c}{|\nabla c|}. \tag{13}$$

The typical time range for corneal angiogenesis experiments is 7 days (Sholley et al., 1984; Thompson et al., 2003), so the time scale T we choose is 1 day, while the time T_0 for a cell to migrate to a steady state is roughly 1 minute. In the numerical simulations, the typical time step is $0.01\,T$ ($= 14.4$ minutes), during which the tip cell has reached a steady state according to (10). Thus, we only consider the steady state of cell elongation as long as the numerical time step is significantly greater than T_0. By combining Eqs. (10) and (13), we obtain

$$u = k_e \frac{\alpha_1}{(c+\alpha_1)^2} \frac{|\nabla c|+\alpha_2}{|\nabla c|+\alpha_3} \frac{\nabla c}{|\nabla c|}, \tag{14}$$

where $k_e = \frac{k_d L_0}{E A_0}$. One example of the profiles of VEGF, its gradient, and the corresponding steady state of cell elongation is shown in Fig. 3.

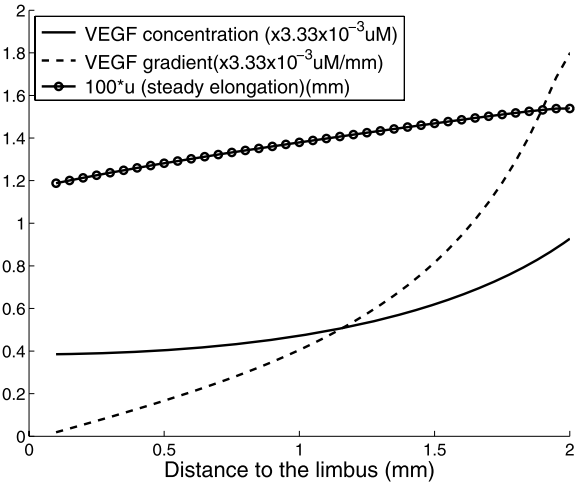

Fig. 3 Example of VEGF, its gradient and steady state u of cell elongation of Eq. (13). The value of u is multiplied by 100 for better view. Solid line: VEGF concentration, dashed line: gradient of VEGF (∇c), and circled line: $100u$. The parameters are the same as in Section 8.

4.2. Multidimensional model: contact guidance

In in vitro and in vivo environments, the migration of cells depends on their adhesion to the extracellular matrix (ECM), the major component of the stroma. The ECM is a mesh-like molecular network composed of fibrous collagen proteins, elastin, adhesive proteins, such as fibronectin and proteoglycans. It has been observed that ECs align themselves along the direction of ECM fibers, a phenomenon called "contact guidance" (Guido and Tranquillo, 1993).

In multidimensional space, to account for contact guidance along ECM fibers, we borrow the idea of conductivity tensor $\mathbf{K}$ from Sun et al. (2005) and modify the chemotactic force to be

$$\mathbf{K} \circ F, \tag{15}$$

then the elongation of tip cell (14) becomes

$$u = k_e \frac{\alpha_1}{(c+\alpha_1)^2} \frac{|\nabla c| + \alpha_2}{|\nabla c| + \alpha_3} \frac{1}{|\nabla c|} \mathbf{K} \circ \nabla c. \tag{16}$$

As in Sun et al. (2005), $\mathbf{K}$ is assumed to be a second order symmetric tensor, and in two-dimensional space it has the form

$$\mathbf{K} = k_{\text{cond}} \begin{pmatrix} a_x^2 & a_x a_y \\ a_y a_x & a_y^2 \end{pmatrix} + \frac{k_{\text{cond}}}{k_a} \begin{pmatrix} a_y^2 & -a_x a_y \\ -a_y a_x & a_x^2 \end{pmatrix}. \tag{17}$$

The parameter $k_{\text{cond}} > 0$ stands for the mechanical response of fibers to the pulling force exerted by the cell. The parameter $k_a \geq 1$ stands for the directional anisotropy of fibers. If $k_a = 1$, then $\mathbf{K}$ becomes $k_{\text{cond}}\mathbf{I}$, where $\mathbf{I}$ is the identity matrix, so it is isotropic at this point. As $k_a \to \infty$, $\mathbf{K}$ tends to be $k_{\text{cond}}\mathbf{a} \otimes \mathbf{a}$. Both k_a and k_{cond} are chosen as random numbers to represent the heterogeneity of the contact guidance. The unit vector $\mathbf{a} = (a_x, a_y)$ is in the direction of the fiber at (x, y) in the ECM, and it is a random variable in space to represent the random orientation of fibers in ECM. Denoting $\mathbf{a}$'s orthogonal vector as $\mathbf{a}^\perp = (-a_y, a_x)$, then Eq. (17) can be rewritten with tensor products as

$$\mathbf{K} = k_{\text{cond}}\mathbf{a} \otimes \mathbf{a} + \frac{k_{\text{cond}}}{k_a}\mathbf{a}^\perp \otimes \mathbf{a}^\perp, \tag{18}$$

which is the generic form in a multidimensional case.

We reinterpret this conductivity tensor model as a simplified version of the mechanical model of the interaction between EC and ECM, where the conductivity tensor mimics the motion the mechanical interaction will provide for the ECs.

5. Nonproliferative extension of sprouts

We single out this topic as a separate section to emphasize its importance. According to the analysis in Sholley et al. (1983b), the nonproliferative migration (or recruitment) of ECs from preexisting vessels contributes to new sprout growth in addition to proliferation, up

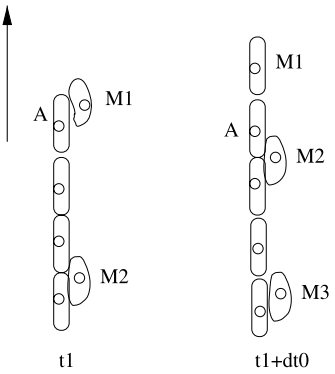

Fig. 4 Diagram of migration of preexisting vessel cells. Cells labeled with M1, M2, and M3 are from preexisting vessels, and are crawling over sprout cells to reach the tip. At time $t_1 + dt_0$, cell M1 replaces cell A as the tip cell.

to 4 days after the onset of angiogenesis. The reason why this process stops after 4 days is unknown, but it is likely related to restrictions of preexisting vessels to maintain integrity.

How a cell from the preexisting vessel is added to a developing sprout still remains a question. The most straightforward way researchers address this issue is to add these new cells to the root, near the base of the existing vessel. If only this type of growth is modeled, then the work of Anderson and Chaplain (1998a, 1998b), with typical Eq. (1), is a simple but good choice. A more complex model is given in Levine et al. (2001a, 2001b), where the motion of cells from preexisting cells is written as an influx condition for the sprouts. However, there is strong evidence that cells can actually crawl along the sprout to the front and even replace the tip cells. This was first indicated in Sholley et al. (1984), where the sprout growth in a cornea cauterized and exposed to 2000 rads irradiation 4 days previously, demonstrates that cells near the tip project pseudopods and layer on each other in a telescoping fashion. More recently, such migration has been observed in vasculogenesis (Szabo et al., 2007), where ECs prefer to migrate along elongated structures. Also, Szabo et al. (2007) provides a discrete mathematical model to simulate this process.

However, the purpose of this paper is not to model the complicated migration of cells from preexisting vessels along sprouts. For the sake of simplicity, we assume the cells from the preexisting vessels migrate along the sprout at a constant speed, so that such cells are added to the tip in constant time interval dt_0 (see Fig. 4). This implies that without proliferation, the sprout extends with a constant speed up to day 4.

6. Maturity and proliferation

ECs have at least two different phenotypes: in most adult endothelium, ECs are in a quiescent state, characterized by little or no proliferation or migration; and near the tip of newly developing blood sprouts, ECs are often actively proliferating and/or migrating. The variation of the quiescent state, or the maturation process, plays an important role in the later stages of angiogenesis. To describe this process, we adapt the model of Plank et al. (2004).

6.1. EC maturation equation

We introduce a new concept for cells: quiescent/maturity level, denoted as m, which is defined as the volume fraction of quiescent cells in a well-defined neighborhood of a cell. The value of m is between 0 and 1, and $m = 0$ corresponds to proliferative cells, while $m = 1$ implies quiescent/mature cells.

Since m denotes the fraction of mature ECs, me is the density of mature ECs, and $e - me$ is the density of immature ECs. According to the experiments of Scharpfenecker et al. (2005), stimulated release of endogenous Ang-2 or overexpression of Ang-2 in ECs perturbs co-culture spheroid integrity, which can be rescued by exogenous Ang-1 and VEGF. Based on this observation, we model the transition from mature cells to immature cells with $\mu_m(me)a_2$, and the transition from immature to mature cells with $b_m(e - me)\frac{a_1}{a_1+\alpha_4}\frac{c}{c+\alpha_5}$, where the Ang-1 and VEGF dependence are modeled by receptor laws. The variables a_1 and a_2 are the concentrations of Ang-1 and Ang-2, respectively. However, as mentioned in Maisonpierre et al. (1997), the destabilizing role by Ang-2 requires a four- to eight-fold excess of Ang-2 to Ang-1, so we multiply by a Heaviside function $H(a_2 - \lambda a_1)$, where λ is a parameter ranging from 4 to 8. Therefore, we obtain the equation for m after canceling e in all terms:

$$\frac{\partial m}{\partial t} = b_m(1 - m)\frac{a_1}{a_1 + \alpha_4}\frac{c}{c + \alpha_5} - \mu_m m a_2 H(a_2 - \lambda a_1), \tag{19}$$

with initial value $m(0) = m_0$. The parameter b_m is the transition rate from immature state to mature state, while μ_m is the transition rate from mature state to immature state. For a newly born daughter cell, the value of m_0 is assumed to be half that of its mother.

6.2. Angiopoietins equations

Ang-1 appears to be expressed mainly by pericytes (Wakui et al., 2006; Suri et al., 1996; Sundberg et al., 2002). For simplicity, we assume the pericyte density is proportional to that of mature cells; therefore, the production of Ang-1 is associated with mature ECs. This handling is the same as Plank et al. (2004). Ang-1 has a uniform background value a_0 as indicated in Maisonpierre et al. (1997). The experiments of Fiedler et al. (2004) show that Ang-2 is released by ECs under stimulation, which are immature cells in our definition. We include diffusion in both the Ang-1 and Ang-2 equations as in Gevertz and Torquato (2006); however, because it is generally believed angiopoietins react in both an autocrine and paracrine manner, and they are primarily localized to ECs or pericytes in rat angiogenesis (Wakui et al., 2006), we will use very small diffusion constants. So we have

$$\frac{\partial a_1}{\partial t} = D_{a_1}\nabla^2 a_1 + b_{a_1} me + \mu_{a_1}(a_0 - a_1), \tag{20}$$

$$\frac{\partial a_2}{\partial t} = D_{a_2}\nabla^2 a_2 + b_{a_2}(1 - m)e - \mu_{a_2} a_2, \tag{21}$$

for any $\mathbf{x} = (x, y) \in \Omega_T$, with initial conditions $a_1(\mathbf{x}, 0) = a_0$, $a_2(\mathbf{x}, 0) = 0$, and no-flux boundary conditions $\frac{\partial a_1}{\partial n}|_{\partial\Omega} = 0$, $\frac{\partial a_2}{\partial n}|_{\partial\Omega} = 0$.

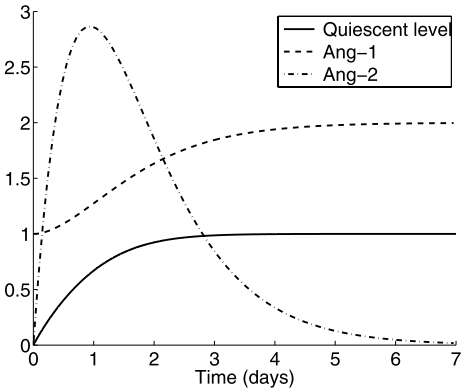

Fig. 5 Evolution of quiescent level, Ang-1 and Ang-2 in a special case: $D_{a_1} = D_{a_2} = 0$ and $e = 1$, $c = 1$. Solid line: maturity level, dashed line: Ang-1, dashdot line: Ang-2. Initial values: $m = 0$, $a_1 = 1$, $a_2 = 0$. Parameters: $b_m = 1$, $\mu_m = 0.1$, $b_{a_1} = 1$, $\mu_{a_1} = 1$, $b_{a_2} = 8$, $\mu_{a_2} = 1$, $\alpha_4 = \alpha_5 = 0$, $\lambda = 8$.

As observed in Scharpfenecker et al. (2005), the storage of Ang-2 in ECs, in combination with the identified rapid endothelial cell functions of Ang-2, implicate a larger production rate b_{a_2} compared to b_{a_1}.

It is preferable that $m = 1$ be the unique steady state of this system because, as shown in the corneal angiogenesis experiments of Cursiefen et al. (2003), pericyte coverage increases with time; after 2 weeks more than 80% of new sprouts are covered with pericytes, and after 36 months 100% of corneal sprouts are covered, and the ECs are quiescent. This is verified as true for our model in the following special case (see the Appendix for proof).

Theorem 1. *Suppose all the parameters are positive in Eqs.* (19), (20), (21), *except* $D_{a_1} = D_{a_2} = 0$, $\alpha_4 = \alpha_5 = 0$ *and* $e = 1$. *If* $\frac{b_m}{\mu_m} > \frac{b_{a_2}}{\mu_{a_2}}$, *then a unique steady state exists and it is* $m = 1, a_1 = a_0 + \frac{b_{a_1}}{\mu_{a_1}}, a_2 = 0$, *and it is asymptotically stable.*

The condition $\frac{b_m}{\mu_m} > \frac{b_{a_2}}{\mu_{a_2}}$ means that the ratio between gain and loss rates of quiescence transitions is larger than that between production and decay rates of Ang-2. The Ang-1 contribution is absent because $\frac{a_1}{a_1+\alpha_4}$, becomes one when $\alpha_4 = 0$. A typical example of the evolution of this system is shown in Fig. 5.

6.3. EC proliferation equation

According to our definition of m, only the immature ECs, with density $(1 - m)e$, have significant proliferative activity, then

$$\frac{\partial e}{\partial t} = \beta_e(1 - m)eH(c - c_p)\frac{c}{c + \alpha_6} - \mu_e(1 - m)e, \tag{22}$$

with initial value $e(0) = e_0$, the normal cell density in nonproliferative vessels. Cell proliferation depends on the concentration of VEGF, and we assume a receptor law $\frac{c}{c+\alpha_6}$.

We further assume the proliferation occurs only when VEGF is higher than a threshold value c_p as in Byrne and Chaplain (1996), Bauer et al. (2007).

Although the logistic growth model is often used, for example, in Plank et al. (2004) and Levine and Nilsen-Hamilton (2006), it is not appropriate to model the proliferation of each individual cell in the sprouts. Equation (22) is designed to simulate the density increase of the cells, and once the density is doubled, it should be divided by two in the cell division process. This phenomenon cannot be modeled by logistic growth. The details of the modeling of this process and its contribution of sprout extension will be described in the Section 7.2.

7. Integrated model of elongation, proliferation and maturation

7.1. Relationship between cell division and sprout elongation

According to the experiments of Bautch's group on rat retina sprouts (Zeng et al., 2007), endothelial cell divisions contribute to both the elongation and thickening of the sprouts, but the majority are oriented toward the long axis of vascular tube formation. From their experiments, about 95% of division cleavage planes are from 45 to 90 degrees perpendicular to the long axis of sprouts. Of the few divisions whose cleavage planes are 0 degree to 45 degrees relative to the long axis, still 30% (3 of 10) of daughter nuclei reorient and move along the long axis. So only 3.5% percent of cell divisions lead to thickening of the sprouts, and the rest to elongating the sprouts. Therefore, in our model, we assume all the cell divisions contribute to the elongation of the sprouts.

7.2. Integrated model

The integrated model combines the migration, proliferation, and maturation processes described above. Each cell divides into two daughter cells once its mass doubles. Immediately after cytokinesis, the new cells are round in shape and easily deformed; therefore, under the chemotactic force, they will be stretched toward the tip, allowing the tip cell to retract and migrate again. By repeating this process, the sprout extends to the source of chemoattractant.

In our model, each individual cell is identified by a single point (x, y) in space, and is assigned the time dependent variables cell mass e and maturity level m. This information, for all the cells in a given sprout, is stored in one array. Therefore, a sprout is represented by an array of discrete points, which forms an irregular line in space due to contact guidance by randomly orientated fibers in the ECM. The concentrations of VEGF (c), Ang-1 (a_1), and Ang-2 (a_2) are defined in the entire space Ω, and are discretized on grid points in numerical simulations.

The time step dt is chosen so that cells elongate to steady state in this time period. Then from time step t_n to $t_{n+1} = t_n + dt$, the entire migration and mitosis process can be described as follows:

- *Migration of tip cells*: the tip cells elongate with displacement (A.3).
- *Migration of cells from preexisting vessels*: up to a fixed time (4 days in our case), one endothelial cell migrating from the preexisting vessels is added to each sprout to replace the tip cell, at every dt_0 time interval.

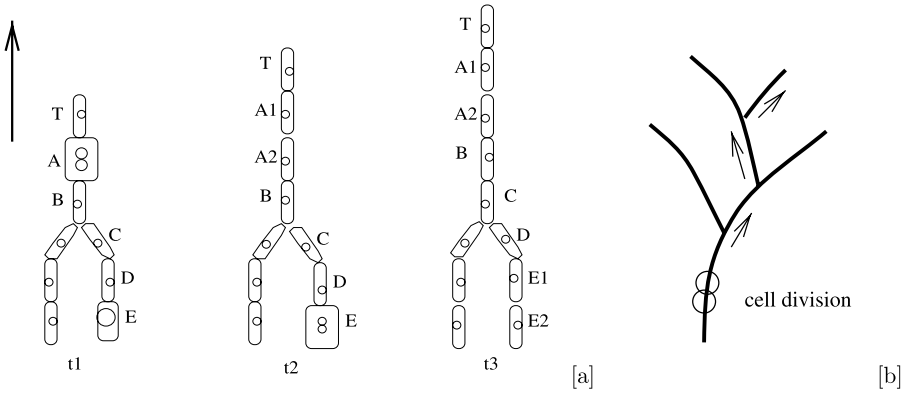

Fig. 6 Sketch of sprout extension in anastomosis (a) and branching (b). In (a), the arrow on the left gives the direction of extension, and both cell A and E are supposed to divide. At t_1, cell A is in mitosis, and it generates cells A1 and A2 at t_2, which allows tip cell T to migrate. At time t_2, cell E is in mitosis, and generates cells E1 and E2 at time t_3, when tip cell T pulls cells A1, A2, B, C, D, and E1 forward. In (b), when a cell division occurs behind branched sprouts, the sprout that will extend is selected randomly and is indicated by arrows.

- *Proliferation*: the maturation Eq. (19) and proliferation Eq. (22) are solved on each cell, and angiopoietin Eqs. (20) and (21) are solved in the whole space.
- *Cell divisions and sprout extension*: if the mass of a cell in the stalk has doubled, then this cell divides into two new cells, and each of them starts with mass and quiescent level equal to half that of their mother cell. One of these new cells takes the position of the old cell, and the other new cell occupies the position of the cell right in front of the dividing cell. Every cell in front of the dividing cell is dragged to replace the cell directly ahead of it, and the tip cell retracts and is ready to elongate again. A schematic of these processes is shown in Fig. 6.

7.3. Sprout extension in anastomosis and branching

Anastomosis (fusion) and branching of capillary sprouts are important morphological features of angiogenesis, and we model them with almost the same rules as Anderson and Chaplain (1998b), thus readers are referred to Anderson and Chaplain (1998b) for details. The difficulty arises in how cell divisions contribute to the extension of sprouts involved in anastomosis and branching.

In anastomosis, only one of two sprouts that fuse together can still extend, so we assume the cell divisions in either of these two sprouts before the fusing point contribute to the elongation of the sprout after the fusing point (see Fig. 6(a)).

In branching, the extension of sprouts is a little more complicated. We assume if one cell divides in the parent sprout, then it can contribute to the extension of only one daughter sprout, which is selected by a 50–50 chance. If the selected daughter sprout has its own branches, then this process is repeated until reaching a tip. Details of this process is illustrated in Fig. 6(b).

7.4. Numerical methods

The reaction Eqs. (19) and (22) are solved by a forward Euler scheme. For time dependent reaction-diffusion Eqs. (20) and (21), a first-order splitting scheme is used, where the reaction is solved by a forward Euler scheme, and the diffusion is solved by a backward Euler scheme.

The diffusion Eq. (7) and diffusion components from splitting are solved by the standard second order continuous piecewise linear finite element methods (FEM), where triangular meshes are constructed from a Cartesian mesh by connecting one pair of diagonal nodes of each small square. One of the advantages of FEM is the symmetry of linear systems, so that fast solvers such as preconditioned conjugate gradient methods can be applied.

Notice that there are two sets of spatial points in our numerical implementations: the points representing the cell positions in the vasculature and the grid points discretizing the equations. Since these two sets of points do not coincide, data has to be transferred between the two sets in computations. First, the data on the sprouts (cell density e and cell quiescent level m) are transferred by extrapolation to the nearby grid points which will be used in the calculations in Eqs. (20) and (21). Suppose a variable ϕ is to be transferred from a cell at point P, as shown in Fig. 7, then we first find the triangle K where P is, then add the value ϕ at P to all the vertices of K. After this process is done for all cells, the final value of ϕ for each grid point is the average of the values added to it. Second, the values of Ang-1, Ang-2 and VEGF are transferred by interpolation to the cell positions which will be used in the calculations in Eqs. (19) and (22). Suppose a variable ψ is to be transferred to the sprout point P in triangle K as shown in Fig. 7, then the value of ψ at P is the weighted sum of ψ at three vertices of K with the weights being the area coordinates of point P in triangle K.

In all simulations, the domain $\Omega = [-2.5, 2.5]^2$ mm^2 is divided into a 200×200 uniform mesh, so the mesh size is 25 μm, comparable to the size of a stretched cell. The time step $dt = 0.01$ (roughly 15 minutes), which is long enough for the tip cells to elongate to the steady state. We compared our simulations to a 100×100 grid, and saw no significant difference in the sprout extension speed, which indicates the consistency and convergence of our numerical methods.

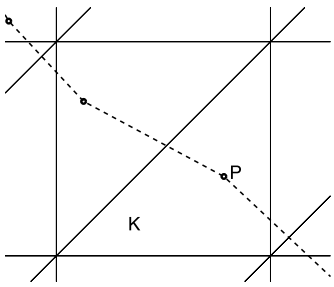

Fig. 7 Illustration of extrapolation and interpolation. Dashed line is the sprout and P represents an endothelial cell that is in triangle K.

7.5. Effect of initial quiescent level

The maturation process (transition to quiescent state) and the initial quiescent level play important roles in our model, as shown in the following theorem in a simple case.

Theorem 2. *If $D_{a_1} = D_{a_2} = 0$, then there exists one critical value $m_c \geq 0$, such that when the initial quiescent level $m_0 > m_c$, the sprout can only extend up to a length provided by the nonproliferative extension of preexisting cells.*

This theorem implies that without diffusion, the sprouts can only extend a limited length if the initial quiescent level is high enough. It can be expected that the same conclusion can be drawn with small angiopoietin diffusion constants.

8. Simulation of corneal angiogenesis

The rat cornea has a thickness of about $0.2 \sim 0.3$ mm, and the part bordered by limbus has a diameter of $4 \sim 5$ mm (Sholley et al., 1984); therefore, it is justifiable to simplify to a two dimensional flat tissue plane.

8.1. Initial conditions for corneal angiogenesis

In the domain described in Fig. 1, we initially assume that there are 90 sprout buds uniformly distributed along the limbus, and each of them is of one cell length $= 0.01$ mm. For the nonproliferative migration of cells from pre-existing vessels, the time interval $dt_0 = 0.15$ days is chosen based on the fact that if there is no proliferation at all, then such migration should give $= 0.58$ mm average vascular length.

In the experiments of Sholley and his collaborators (Sholley et al., 1983a, 1983b, 1984, Sholley and Wilson, 1987), different doses (from 500 rads to 8000 rads) of X-ray radiation were applied to pre-existing blood vessels in the corneal limbus to suppress the DNA synthesis of ECs, thus stalling the proliferation. Increasing the irradiation led to more cellular damage and less proliferation (Sholley et al., 1983a). Therefore, we interpret the irradiation dose as the initial condition for the quiescent level.

8.2. Nondimensionalization and parameter estimates

In order to compare with the rat corneal angiogenesis experiments of Sholley et al. (1984) and Thompson et al. (2003), we choose the characteristic length scale to be the distance from limbus to the lesion $L = 2$ mm, and the characteristic time scale $T = 1$ day. We denote EC density in the normal sprout as e_0, VEGF concentration at the tumor boundary as c_0, and Ang-1 background concentration as a_0. Let $\mathbf{x}' = \mathbf{x}/L$, $t' = t/T$, $c' = c/c_0$, $u' = u/L$, $a_1' = a_1/a_0$, $a_2' = a_2/a_0$, and $e' = e/e_0$, then the equations in our model become (after dropping primes of $\mathbf{x}', t', c', u', a_1', a_2', e'$):

$$\frac{\partial c}{\partial t} = D_c' \nabla^2 c - \mu_c' c - \frac{k_{\max}' c e}{k_n' + c}, \tag{23}$$

$$u = k_e' \frac{\alpha_1'}{(c+\alpha_1')^2} \cdot \frac{|\nabla c| + \alpha_2'}{|\nabla c| + \alpha_3'} \cdot \frac{1}{|\nabla c|} \mathbf{K} \circ \nabla c, \tag{24}$$

$$\frac{\partial m}{\partial t} = b_m'(1-m) \frac{a_1}{a_1 + \alpha_4'} \cdot \frac{c}{c+\alpha_5'} - \mu_m' m a_2 H(a_2 - \lambda a_1), \tag{25}$$

$$\frac{\partial a_1}{\partial t} = D_{a_1}' \nabla^2 a_1 + b_{a_1}' m e + \mu_{a_1}'(a_0 - a_1), \tag{26}$$

$$\frac{\partial a_2}{\partial t} = D_{a_2}' \nabla^2 a_2 + b_{a_2}'(1-m)e - \mu_{a_2}' a_2, \tag{27}$$

$$\frac{\partial e}{\partial t} = \beta_e'(1-m) e H(c - c_p') \frac{c}{c+\alpha_6'} - \mu_e'(1-m)e, \tag{28}$$

with conditions

$$\begin{aligned} &c|_{\partial\Omega_T} = 1, \qquad \left.\frac{\partial c}{\partial n}\right|_{\partial\Omega} = 0, \qquad m(0) = m_0, \qquad a_1(0) = 1, \\ &a_2(0) = 0, \qquad e(0) = 1. \end{aligned} \tag{29}$$

The definitions of dimensionless parameters (with primes) are listed in Table 2.

Whenever possible, the parameters are chosen from existing literature. For EC maturation and angiopoietins, all the parameters are unknown, so we have to estimate them according to the requirement of desired properties of angiopoietins, as in Plank et al. (2004) and Gevertz and Torquato (2006). The VEGF threshold value for EC proliferation, c_p, is not available in the literature, therefore, it is simply set to be one-tenth of the reference VEGF value, c_0. The values of all parameters are given in Tables 1 and 2.

8.3. Normal growth

The results of the simulation with normal growth (0 rads irradiation) are shown in Fig. 8. The vasculature reaches halfway across the domain at day 4 (Fig. 8(a)), reaches the lesion at day 7 (Fig. 8(b)), and gives rise to the brush-border effect. The quiescent level of the cells is higher at the roots than that at the tips on both days 4 and 7, which is the same as the distribution of Ang-1, but opposite to Ang-2. Note that the spatial distributions of Ang-1 and Ang-2 in Fig. 8 agree with the patterns of Ang-1 and Ang-2 transcripts in the vascular remodeling of rat ovary (Maisonpierre et al., 1997), respectively.

To investigate the evolution of these quantities more carefully, we select one specific sprout, and the results are shown in Fig. 9. At day 4, the sprout reaches a length of 1.08 mm, and all the cells have a relatively low and uniform quiescent level and Ang-1 concentration, but have a very high Ang-2 concentration, thus they are actively proliferating. At day 7, the sprout reaches the lesion and the cells near the limbus are of high quiescent level (close to 1), consistent with the high value of Ang-1 and low value of Ang-2. The cells in the front still maintain low values of quiescence and Ang-1 but high level of Ang-2, thus proliferate actively.

As expected, proliferation mainly occurs near the tips. Figure 10(a) shows the percentage of cell divisions that occur within 0.5 mm distance of the leading edge of the sprout,

Table 1 Dimensional parameters and their values

Parameters	Values	Sources
Length scale, L	2 mm	Sholley et al. (1984)
Time scale, T	1 day	Sholley et al. (1984)
EC reference density, e_0	3.32×10^{-8} μM	Sholley et al. (1984), Karl et al. (2005)
VEGF reference concentration, c_0	3.33×10^{-3} μM	Bauer et al. (2007)
Angiopoietin reference concentration, a_0	10^{-3} μM	Plank et al. (2004)
VEGF diffusion constant, D_c	50.88 mm^2 per day	Sherratt and Murrat (1990)
VEGF decay rate, μ_c	15.60 per day	Serini et al. (2003)
VEGF maximum uptake rate, $k_{\max}$	3.68×10^6 per day	Jain et al. (2008), Mac Gabhann and Popel (2004), Wang et al. (2002)
VEGF half saturation constant, k_n	8.85×10^{-4} μM	Jain et al. (2008), Mac Gabhann and Popel (2004), Wang et al. (2002)
Ang-1 diffusion constant, D_{a_1}	1.67×10^{-5} mm^2/h	
Ang-2 diffusion constant, D_{a_2}	1.67×10^{-6} mm^2/h	
Ang-1 production rate, b_{a_1}	3×10^4 per day	
Ang-1 decay rate, μ_{a_1}	0.1 per day	
Ang-2 production rate, b_{a_2}	1.2×10^6 per day	
Ang-2 decay rate, μ_{a_2}	4.0 per day	
EC proliferation rate, β_e	0.96 per day	Sherratt and Murrat (1990)
EC death rate, μ_e	0.005 per day	Cho et al. (1997)
EC maturation rate, b_m	0.4 per day	
EC activation rate, μ_m	9.0×10^{-5} μM per day	
EC maturation parameter, λ	4	Maisonpierre et al. (1997)
EC elongation parameter, k_e	2.66×10^{-3} mm·μM	
VEGF threshold value for EC proliferation, c_p	3.33×10^{-4} μM	
EC elongation parameter, α_1	4.0×10^{-2} μM	
EC elongation parameter, α_2	10^{-2} μM per mm	
EC elongation parameter, α_3	1.67×10^{-3} μM per mm	
EC maturation parameter, α_4	10^{-3} μM	
EC maturation parameter, α_5	3.33×10^{-4} μM	
EC proliferation parameter, α_6	3.33×10^{-5} μM	
ECM conductivity parameter, k_{cond}	$^*N(1, 0.1)$	Sun et al. (2005)
ECM anisotropy parameter, k_a	$^*U(1, 20)$	Sun et al. (2005)

$^*N(p, q)$ means normal random variable with mean p and variance q
$^*U(p, q)$ means uniform random variable between p and q

which is qualitatively consistent with that of (Sholley et al., 1984) (Fig. 2(a)). From day 4 to day 7, the percentage decreases from 60% to 55% because the actively dividing (proliferating) region enlarges toward the rear. This is verified from Fig. 10(b), where the regions of actively dividing cells (>10 divisions) enlarge from 1.0 mm to 1.5 mm within the tip from day 4 to day 7. This indicates that although the cells toward the rear exhibit less proliferative activity as they mature, they are still important contributors to sprout extension.

Table 2 Nondimensionalized parameters and their values

Parameters	Values	Parameters	Values
$D_c' = D_c T/L^2$	12.72	$\mu_{a_2}' = \mu_{a_2} T$	4
$\mu_c' = \mu_c T$	15.60	$\beta_e' = \beta_e T$	1
$k_{\max}' = k_{\max} T \frac{e_0}{c_0}$	36.8	$\mu_e' = \mu_e T$	0.005
$k_n' = \frac{k_n}{c_0}$	0.266	$k_e' = k_e/(Lc_0)$	0.4
$D_{a_1}' = D_{a_1} T/L^2$	10^{-4}	$c_p' = c_p/c_0$	0.1
$D_{a_2}' = D_{a_2} T/L^2$	10^{-5}	$\alpha_1' = \alpha_1/c_0$	12
$b_m' = b_m T$	0.4	$\alpha_2' = \alpha_2 L/c_0$	0.6
$\mu_m' = \mu_m T/a_0$	0.09	$\alpha_3' = \alpha_3 L/c_0$	1
$b_{a_1}' = b_{a_1} T e_0/a_0$	1	$\alpha_4' = \alpha_4/a_0$	1
$\mu_{a_1}' = \mu_{a_1} T$	0.1	$\alpha_5' = \alpha_5/c_0$	0.1
$b_{a_2}' = b_{a_2} T e_0/a_0$	40	$\alpha_6' = \alpha_6/c_0$	1

The comparison of vasculature extension speed among various cases is shown in Fig. 11, where good agreement between simulations and experimental results are achieved.

8.4. Modulation of proliferation: angiopoietins vs. VEGF

In our model, VEGF uptake mediates EC proliferation (Eq. (22)); therefore, the free VEGF concentration is reduced as the sprout extends toward the lesion, as shown in Fig. 12. This result is consistent with the prediction of Cellular Potts model (Bauer et al., 2007), and is also consistent with the rat subcutaneous angiogenesis (Wakui et al., 2006) and corneal angiogenesis (Amano et al., 1998), where it is observed that the VEGF mRNA concentration drops sharply with the progression of angiogenesis.

EC proliferation depends on the concentration of VEGF, and it is therefore expected that the gradient of VEGF concentration may also play a role in localizing proliferation to the leading edge of the vasculature. The gradient of VEGF is caused by the natural decay and uptake by ECs. To compare the differential effects the maturation process and the VEGF profile on where proliferation occurs, we perform three simulations: maturation without VEGF uptake; VEGF uptake without maturation; and without both maturation and VEGF uptake. The results, shown in Fig. 13, confirm our intuition. With the parameters chosen, both the maturation process and the uptake of VEGF alone can localize the proliferation to the front, but the prediction of sprout extension is too fast compared with experiments. Therefore, the localization of proliferation is more likely caused by the combination of these two mechanisms.

8.5. Effects of irradiation

In the case of 2000 rads irradiation, the initial quiescent level is set at $m_0 = 0.5$ and the results are shown in Fig. 14. At day 7, the sprouts extend to length 0.74 mm, and most cells are quiescent (82% cells are of $m = 1$). The simulation after day 7 shows that the vasculature extends to a steady state which does not reach the tumor (see Fig. 16(a)).

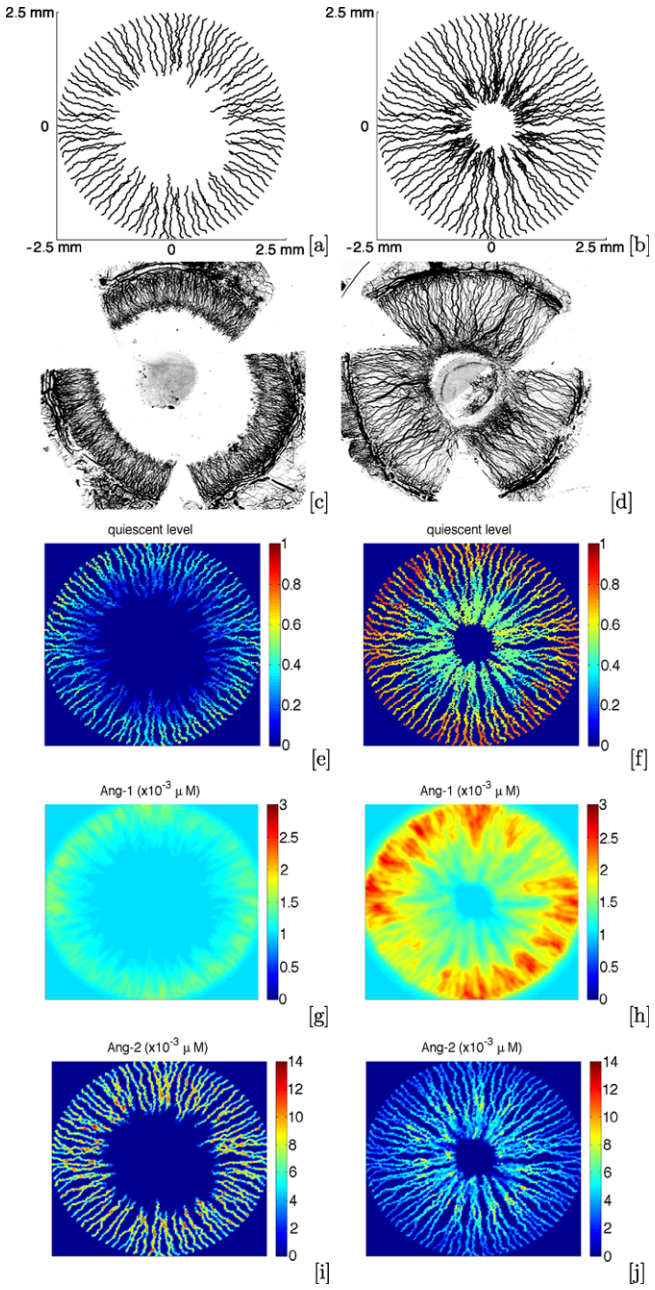

Fig. 8 Simulations of normal growth. Left column: Day 4. Right column: Day 7. (a) At day 4, there are 90 sprouts with average length 1.06 mm. (b) At day 7, there are 336 sprouts with average length 1.84 mm. Second row ((c) and (d)): experimental results (reprinted from Thompson et al., 2003 with permission). Third row ((e) and (f)): quiescent level. Fourth row ((g) and (h)): Ang-1 concentration. Fifth row ((i) and (j)): Ang-2 concentration.

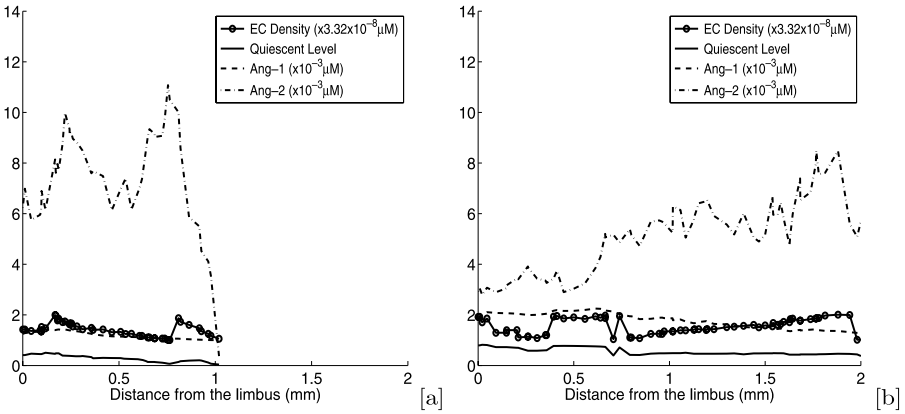

Fig. 9 Quantities on a sprout at day 4 (a) and day 7 (b): EC density (circled line), quiescent level (solid line), Ang-1 (dashed line) and Ang-2 (dashdot line).

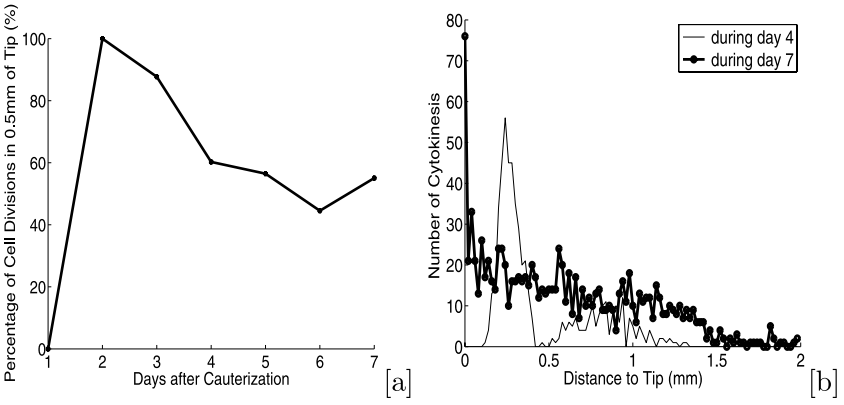

Fig. 10 (a) Percentage of cell divisions within 0.5 mm of leading edge. (b) Distribution of cell divisions at day 4 (thin line) and day 7 (thick line with dots) after cauterization.

In the case of 8000 rads irradiation, the initial quiescent level is set at $m_0 = 0.8$ and the results are shown in Fig. 15. At day 7, the sprouts extend to a steady state length 0.58 mm, and all cells are quiescent ($m = 1$). In this case, each sprout has 28 cells on average, and only 2 of them are generated from proliferation; thus, the main contribution to the vascular extension is the nonproliferative migration of preexisting ECs. In both cases, the Ang-1 concentration is very high in the entire vasculature region and the Ang-2 concentration is low, which explains why the cells are mostly quiescent.

The effect of irradiation, for a large range of doses, on the sprout growth is demonstrated in Fig. 16. When the initial quiescent level m_0 increases from 0 to 1.0, the sprout extension length on day 7 decreases, illustrated by the red solid curve in Fig. 16(a), which qualitatively matches the experimental results shown in Fig. 16(b) from Sholley et al. (1984). The limiting value is achieved when $m_0 = 1$ and the corresponding sprouts are

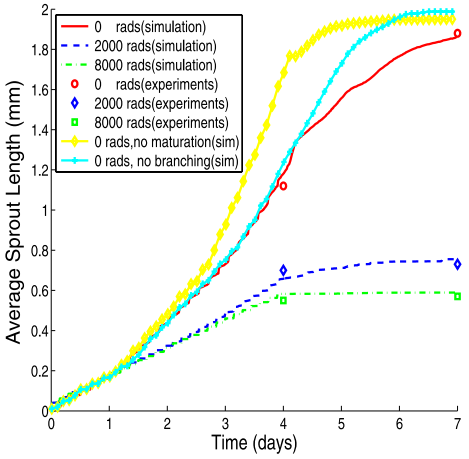

Fig. 11 Average vascular extension length vs. time. Solid line: no irradiation with branching; dashed line: 2000 rads; dashdot line: 8000 rads; solid with diamond: no maturation process; solid with +: no branching. Experiments: circles for 0 rads, diamonds for 2000 rads and squares for 8000 rads.

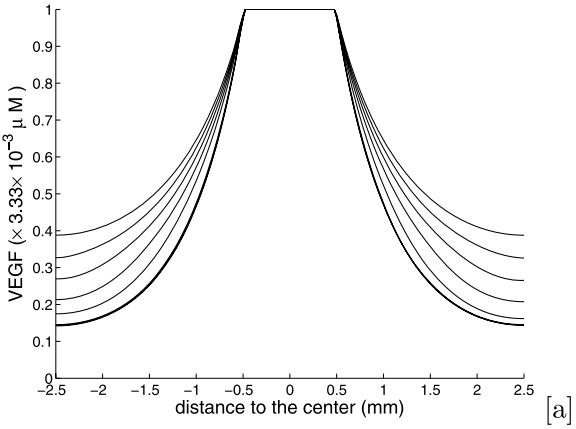

Fig. 12 VEGF concentration across a centerline at day 0, 1, . . . , 7 (from top to bottom).

formed only by nonproliferative cells. The decrease of sprout length is due to the fact that more cells transition to the quiescent state $m = 1$ (blue dashed curve in Fig. 16) and, therefore, cannot proliferate to extend the sprouts. The green dashdot curve in Fig. 16 shows the steady state sprout length when time goes to infinity. A steady state length of 2 mm means that the sprouts have reached the lesion. When the initial quiescent level is no less than 0.5, the steady state length is finite and less than 2 mm, which implies that the sprouts can never reach the injury. This result is consistent with the prediction of Theorem 2.

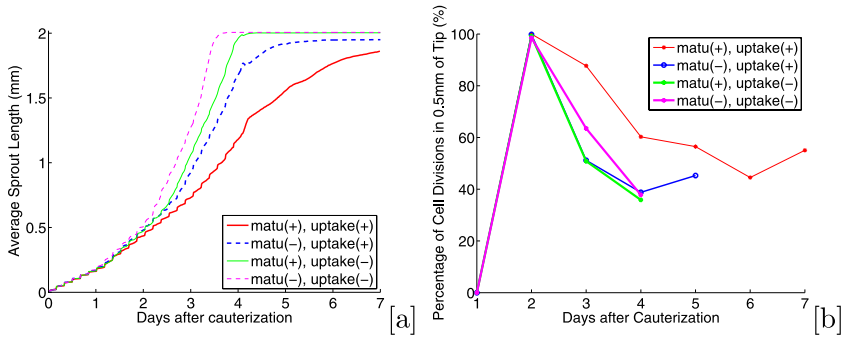

Fig. 13 Comparison of sprout extension speed and proliferation localization in four cases: normal growth with maturation and uptake of VEGF; growth without maturation but with uptake of VEGF; growth with maturation but without uptake of VEGF; and, growth without both. (a) Sprout extension length vs. time. (b) Proliferation percentage within 0.5 mm of the tip.

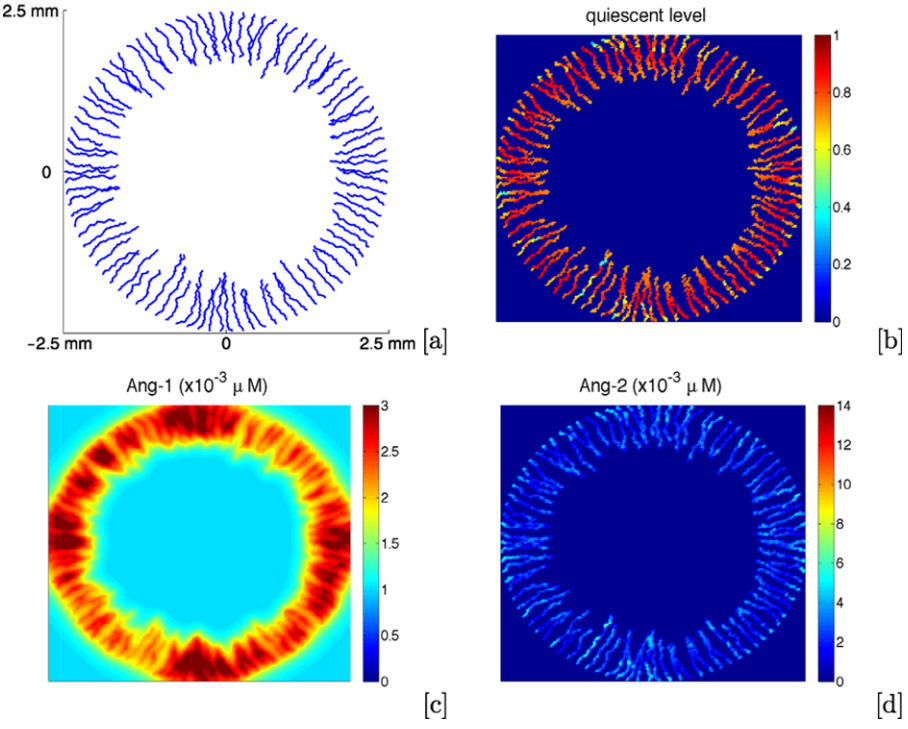

Fig. 14 Simulation results at day 7 of angiogenesis under initial quiescent level $m_0 = 0.5$, corresponding to 2000 rads irradiation: (a) vasculature, (b) quiescent level, (c) Ang-1 concentration, and (d) Ang-2 concentration. Average sprout extension length is 0.74 mm, and 82% cells are of $m = 1$.

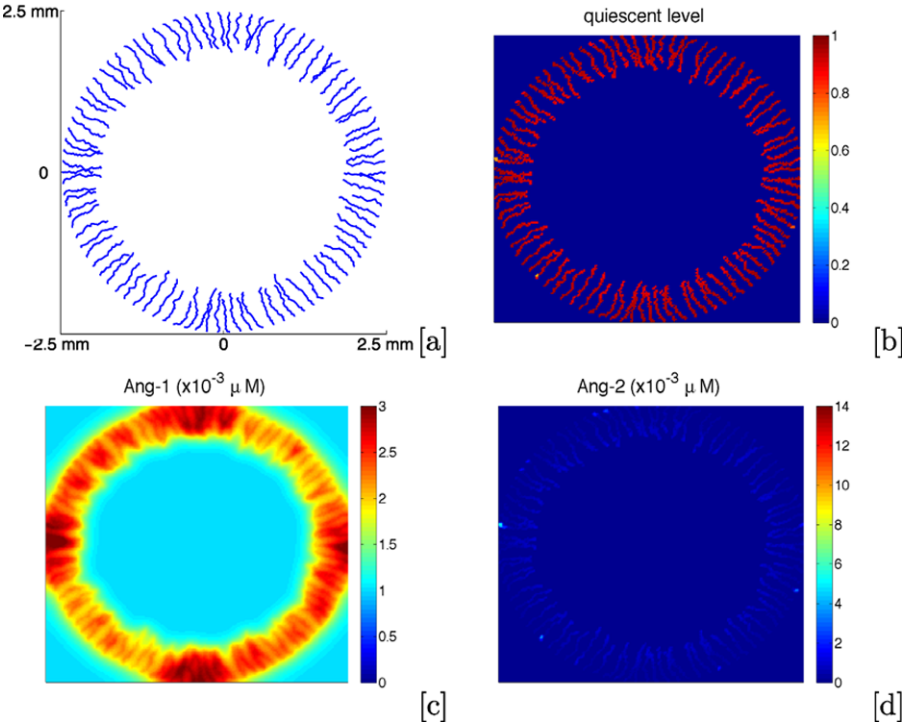

Fig. 15 Simulation results at day 7 of angiogenesis under initial irradiation 8000 rads: (a) vasculature, (b) quiescent level, (c) Ang-1 concentration, and (d) Ang-2 concentration. Average sprout extension length is 0.58 mm, and 100% cells are of $m = 1$.

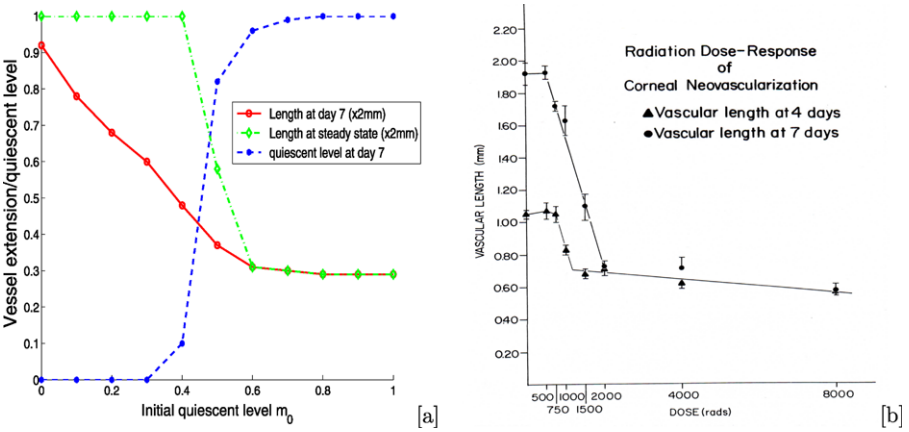

Fig. 16 (a) Numerical simulation of the effect of initial quiescent level on sprout growth. Red solid curve is the average sprout length at day 7 after onset of angiogenesis, blue dashed curve is the percentage of cells of the quiescent level $m = 1$ at Day 7, and green dashdot curve is the steady state sprout length. (b) Experimental results of irradiation right before cauterization on sprout growth. This figure is reprinted from Sholley et al. (1983b) with permission.

8.6. *Effect of Ang-2 inhibition*

Because Ang-2 stimulates angiogenesis and prevents new sprouts from maturing (Fiedler et al., 2006), the inhibition of Ang-2 may have antiangiogenenic potential, as demonstrated by White et al. (2003). In the experiments of White et al. (2003), a nuclease-resistant RNA aptamer (11-1.41), that binds Ang-2 but not Ang-1, was delivered to the rat corneal micropocket angiogenesis assay and as a result, basic fibroblast growth factor (bFGF) mediated neovascularization was completely or partially inhibited, compared to the corneas treated with the Scramble aptamer, whose ability to bind Ang-2 is disrupted. The complete inhibition may have been due to the prevention of the onset of angiogenesis, which it is not the topic of this paper as we are concerned with the later stages of sprout development. However, there is increasing evidence that Ang-2 plays a crucial role in the activation of angiogenesis (Fiedler et al., 2006; White et al., 2003; Oliner et al., 2004), and more detailed modeling of this important area, including the molecular level signaling pathways, is under investigation now (Jackson and Zheng, 2009). Here, we study how the binding of Ang-2 to aptamer can partially inhibit sprout extension. Because the binding of Ang-2 to aptamer reduces the amount of Ang-2 available to ECs, we model this binding effect by an increase in the Ang-2 decay rate parameter μ_{a_2} in Eq. (21). The value of μ_{a_2} is increased from 4 per day, as in the normal growth, to 40 per day and the results at day 6 are shown in Fig. 17.

Our results show that the average sprout length at day 6 is about 1.23 mm, which is about 70% of the length shown in Section 8.3 for the normal growth. This ratio is the same as in the experiments of (White et al., 2003). Comparing Fig. 17 with Fig. 8, we find the concentration of Ang-2 is significantly reduced, while Ang-1 levels are roughly the same. Note however, that the maturity or quiescent level is higher and, therefore, the sprout extension is slower. Indeed, the sprouts become completely quiescent before they reach the tumor (data not shown). The experimental result with partially inhibited vasculature at day 6 after the onset of angiogenesis is shown in Fig. 17(e) (left) with a comparison to the normal growth (right). Therefore, our model qualitatively captures the Ang-2 inhibition effect.

8.7. *Effects of branching and anisotropy*

Data concerning the anisotropy of ECM and the occurrence of anastomoses and branching in corneal angiogenesis are not currently available; therefore, we can only predict the effects of branching and ECM anisotropy with our mathematical model. If one sprout branches into two daughter sprouts, then one cell division before the branch point gives rise to the extension of only one daughter sprout, which is selected randomly in our algorithm. Therefore, the contribution of such divisions to sprout extension is halved on average, which implies slower sprout extension in the case of branching. For example, in the case of normal growth, if the branching process is turned off, then the sprouts extends faster (see comparison of speed in Fig. 11). But the brush-border effect is not so remarkable compared to the case with branching (Fig. 18 vs. Fig. 8(b)).

Anisotropy of ECM affects the sprout extension speed and the vasculature morphology. As shown in Fig. 19(a), the higher the anisotropy, the slower the sprout's extension; and when k_a is chosen as the $U(1, 20)$ ($U(a, b)$ represents the uniform distribution between a and b), the sprout extension lengths agree with experiments (Sholley et al., 1984)

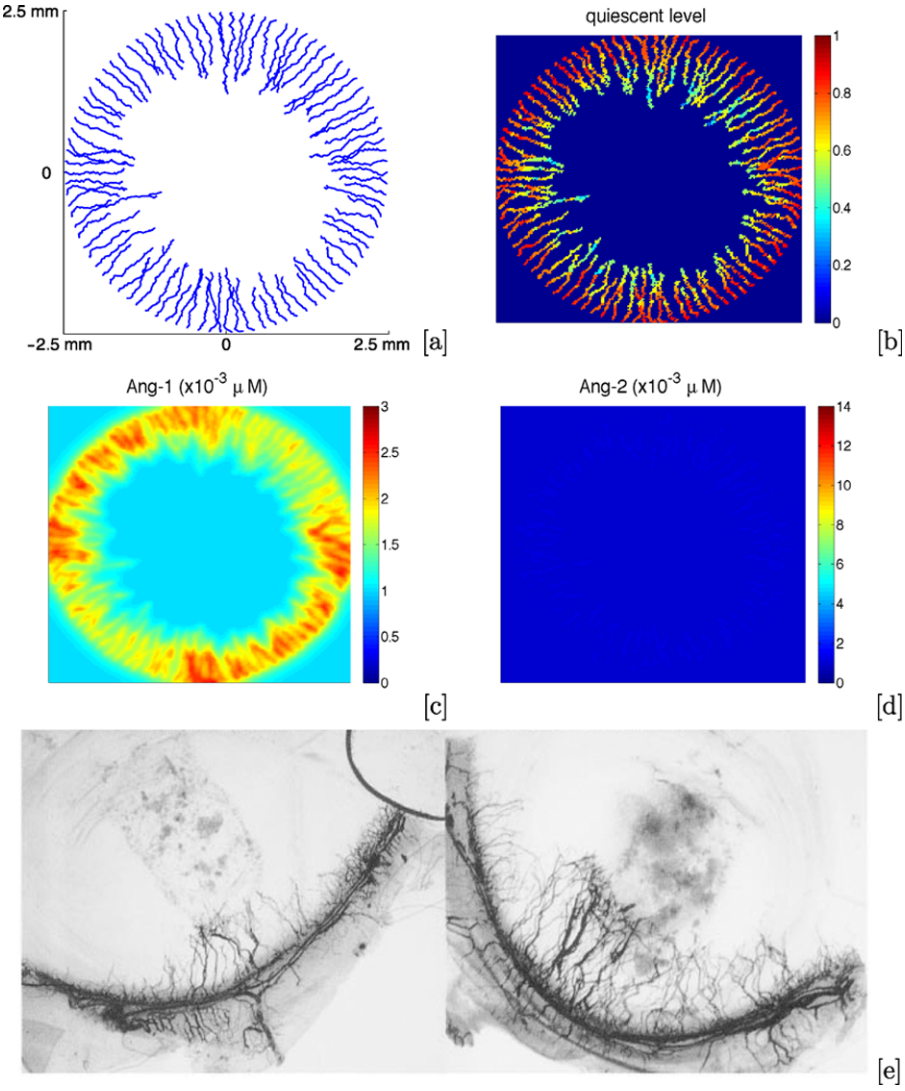

Fig. 17 Ang-2 inhibition: simulation results at day 6 (a, b, c, d) and experimental results at day 6 (e). In the simulation, $\mu_{a_2} = 40$ per day, compared with $\mu_{a_2} = 4$ per day, which is the normal case shown in Fig. 8. (a): at day 6, there are 187 sprouts with average length 1.12 mm. (b): quiescent level. (c): Ang-1 concentration. (d): Ang-2 concentration. (e) Experimental results at day 6 after the onset of angiogenesis: the left picture shows the cornea treated with the 11-1.41 aptamer, while the right picture shows the cornea with the Scramble aptamer (reprinted from White et al., 2003 with permission. Copyright (2003) National Academy of Sciences, USA).

at day 4 and day 7. When k_a is chosen to be $U(1, 2)$, the ECM is almost isotropic and the sprouts are very straight in morphology (Fig. 20(a)); therefore, the extension is very fast. With higher anisotropy, the ECs migrate with more deviation from the radial direc-

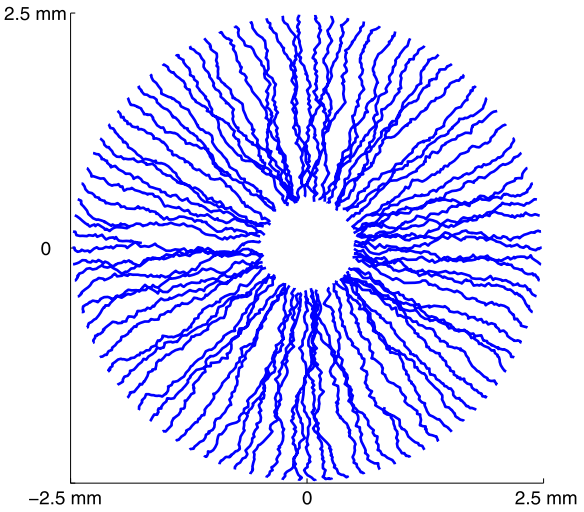

Fig. 18 Vessels at day 7 without branching (compared to Fig. 8(b)).

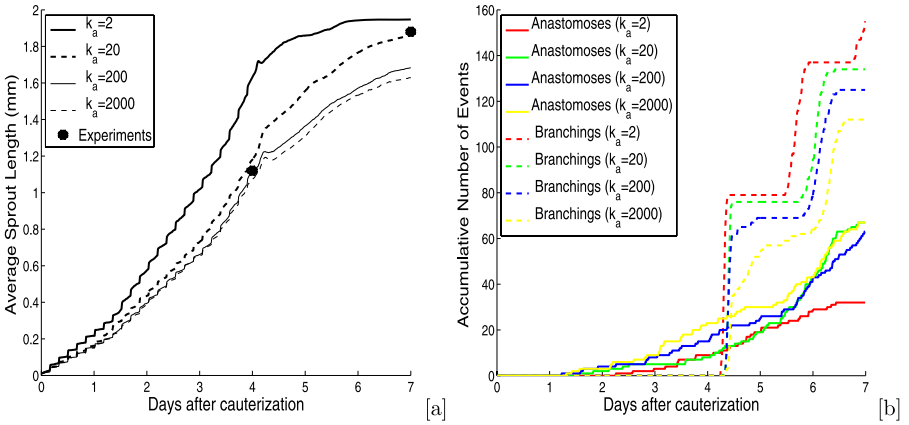

Fig. 19 (a) Sprout extension length vs. time for different values of the anisotropy parameter, k_a. Moving from top to bottom k_a increases from $U(1,2)$ to $U(1,2000)$. The two dots are experimental data points from Sholley et al. (1984). (b) Accumulative numbers of anastomosis and branching events for different values of k_a. Red curves: $k_a = U(1,2)$, green curves: $k_a = U(1,20)$, blue curves (representing normal growth): $k_a = U(1,200)$, and yellow curves: $k_a = U(1,2000)$. Solid and dashed curves depict the number of anastomosis and branching events, respectively.

tion; therefore, the sprouts are more tortuous ($k_a = U(1,2000)$ as shown in Fig. 20(b)), which in turn slows down the extension speed. The vasculature in the case of smaller anisotropy also exhibits fewer anastomoses because sprouts have less chance to merge, and more branching because sprouts extend faster and are exposed to higher concentra-

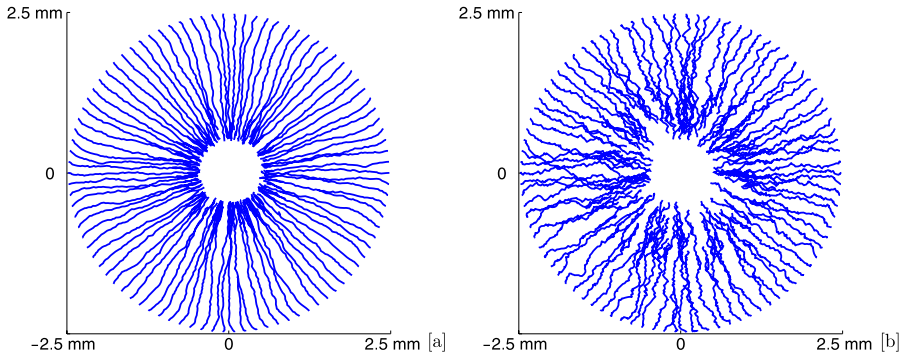

Fig. 20 Sprout morphologies at day 7 with different anisotropy parameter k_a. (a) $k_a = U(1, 2)$, 263 sprouts with average length 1.94 mm. (b) $k_a = U(1, 2000)$, 206 sprouts with average length 1.62 mm. For comparison with normal growth case, see Fig. 8(b).

tions of VEGF sooner. Recall the branching probability is proportional to VEGF concentration as shown in Anderson and Chaplain (1998b).

9. Discussion

The main purpose of this work is to resolve two problems in angiogenesis—we aim to understand why proliferation is necessary for developing sprouts to reach the chemoattractant source, and why this proliferation is concentrated at the leading edge of the emerging vasculature. Solving these two problems requires an in-depth understanding of the mechanisms of cell elongation, proliferation, and maturation. The paucity of experimental data and the complexity of the biological nature of angiogenesis represent a significant challenge for mathematical modeling. We met this challenge by proposing a cell-based model for vascular extension and by investigating these mechanisms with an emphasis on the relationships between them. Our mathematical predictions are in very good agreement with corneal angiogenesis experiments.

Our model contains two main features. The first is a viscoelastic spring model of the ECs, which are tightly connected by cell-cell adhesion, in a developing sprout. Thus, the whole vasculature is regarded as a spring network. Cells in the sprout have two different phenotypes: migrating tip cells and proliferating stalk cells. The tip cell generates the chemotactic force that drags the trailing sprout, but only a limited distance dictated by elasticity. However, if a new cell is born by proliferation, the tip cell can drag the sprout forward again, but to another finite distance still limited by elasticity. Therefore, elasticity restricts cell length to a finite size, and together with adhesion, ensures that sprouts can only extend to a limited length without proliferation.

Compared with other cell-based models (Peirce et al., 2004; Bauer et al., 2007; Qutub and Popel, 2009), our model represents each cell, including tip cells and stalk cells, by a single spatial point. Although it does not take into account the shape of the cells, our model captures the basic morphological features of cells such as location, length, and orientation. More importantly, it provides a far simpler framework which is very easy to

implement. Moreover, the entire model can be directly extended to three dimensions with very few modifications.

The second main feature is the introduction of the quiescent transition (maturation) process modulated by angiopoietins, which is adapted from the work of Plank et al. (2004). Based on our results, we conclude that the maturation process can explain why the cells at the leading edge of vasculature are more proliferatively active than the cells behind them. However, this does not attenuate the important role of the bioavailability of VEGF in the localization of proliferation. Indeed, our results suggest that both mechanisms contribute to the concentration of the proliferation on the leading edge.

This work considered the regulation of EC proliferation by angiopoietins, and confirms that the inhibition of Ang-2 binding to the Tie-2 receptor has therapeutic potential for anti-angiogenesis treatment. Indeed, the angiopoietins are crucial in many other aspects of angiogenesis, including EC activation, migration, and permeability (Augustin et al., 2009), which will be addressed in our future work (Jackson and Zheng, 2009).

It is also relevant to note that we described the contribution of proliferating cells to sprout extension in a temporally discontinuous manner, which occurs only when cells divide. The analysis of Sholley et al. (1987) points out that simply the increase of cell size can contribute to sprout extension. As they mentioned, a small number of surviving ECs in an irradiated cornea might result in the same vascular length as a larger number of cells in an unirradiated cornea because, although the irradiated cells are stalled from entering DNA synthesis process, they can still grow longer under the dragging force. This mechanism indicates that the contribution of proliferation to sprout extension is a continuous process, that is, the sprout elongates as soon as cells grow. A continuous model of sprout extension based on EC migration and proliferation is under investigation now (Jackson and Zheng, 2009).

The manner in which our model currently handles nonproliferative recruitment of cells from the parent vessels is ad hoc. All of our assumptions, including how often the cells are recruited, are highly dependent on the specific tissue and physiological environment. In some special cases, for instance, when the preexisting vessel is sufficiently close to the lesion, solely nonproliferative cell recruitment is adequate to ensure that vessels reach the lesion. However, most experimental evidence shows that proliferative migration is essential for the success of angiogenesis.

In our work, we have kept the modeling mechanisms and equations to a minimum. For example, the EC-ECM interactions play important roles in angiogenesis but we considered only contact guidance by ECM. In addition, we have used only receptor laws to represent all of the ligand-receptor kinetics. Nevertheless, our results showed that these simplifications capture the most critical information, and enable us to concentrate on the relationships between proliferation, migration, and maturation in the sprout extension.

In summary, angiogenesis has proven to be far too complex a problem to be described in a single mathematical modeling framework, especially given that a large amount of information is still unknown. We envision our model as an intermediate step to incorporate reasonable elements from previous works and provide a basis for future improvements. For example, the VEGF-Bcl2-CXCL8 signaling pathway that mediates EC survival is a natural refinement of this work. Our ultimate goal is to combine this model with tumor growth simulators to predict antiangiogenesis treatment, based on the work of Jain et al. (2008).

Acknowledgements

This work is supported by the James S. McDonnell Foundation. The authors thank Dr. Milton Sholley for his invaluable assistance in the discussion of the angiogenesis process and for providing us important experimental data.

Appendix: Derivation of Spring model in one dimensional space

As shown in Munevar et al. (2001), an endothelial cell can be divided into two portions with distinct functions in migration: lamellipodia as towing zone, and main cell body as cargo zone. Denote $[0, L_0]$ as the main cell body, $(L_0, L_0 + L_1]$ as lamellipodia, and $u(x,t)$ as displacement for $x \in [0, L_0 + L_1]$. The one dimensional viscoelastic model can be written as (cf. Larripa and Mogilner, 2006)

$$\beta \frac{\partial u}{\partial t} = h \frac{\partial \sigma}{\partial x}, \tag{A.1}$$

$$\sigma = E \frac{\partial u}{\partial x} + \mu \frac{\partial^2 u}{\partial t \partial x} + \tau, \tag{A.2}$$

where E is the Young's modulus, μ is the viscosity coefficient, β is the friction between EC and ECM, τ is the internal stress produced by actin assembly, and h is the cell height. Integrating over lamellipodia $(L_0, L_0 + L_1]$, we obtain

$$\int_{L_0}^{L_0+L_1} \beta \frac{\partial u}{\partial t}\, dx = h\big(\sigma(L_0 + L_1) - \sigma(L_0)\big). \tag{A.3}$$

In the elongation process, we assume lamellipodia keep the same length, that is, the displacement in lamellipodia is uniform, then for any $x \in (L_0, L_0 + L_1]$,

$$\frac{\partial u}{\partial x} = 0, \tag{A.4}$$

$$\frac{\partial u}{\partial t}(x,t) = \left.\frac{\partial u}{\partial t}\right|_{L_0+}. \tag{A.5}$$

Equations (A.2) and (A.4) imply $\sigma(L_0 + L_1) = \tau(L_0 + L_1)$. In the main cell body, we assume a linear displacement, that is, for $x \in [0, L_0]$, $u(x,t) = u(L_0,t)x/L_0$, then $\sigma(L_0) = \tau(L_0) + E\frac{u(L_0,t)}{L_0} + \frac{\mu}{L_0}\frac{du(L_0,t)}{dt}$ and $\frac{\partial u}{\partial t}|_{L_0-} = \frac{du(L_0,t)}{dt}$. The continuity of displacement speed, $\frac{\partial u}{\partial t}|_{L_0+} = \frac{\partial u}{\partial t}|_{L_0-}$, and (A.5) imply that $\frac{\partial u}{\partial t}(x,t) = \frac{du(L_0,t)}{dt}$ for $x \in (L_0, L_0 + L_1]$.

With these relations, (A.3) becomes

$$L_1 \beta \frac{du(L_0,t)}{dt} = h\left(\tau(L_0 + L_1) - \tau(L_0) - E\frac{u(L_0,t)}{L_0} - \frac{\mu}{L_0}\frac{du(L_0,t)}{dt}\right). \tag{A.6}$$

Multiply the above equation with cell width W, and denote $A_0 = L_0 W$ as the cell cross-section area and $A_1 = L_1 W$ as the contact area between lamellipodia and ECM.

Define $F = A_0(\tau(L_0 + L_1) - \tau(L_0))$ as the protrusion force generated by lamellipodia and $u(t) = u(L_0, t)$ as the displacement of bulk cell body at time t, we then obtain

$$A_1\beta\frac{\partial u}{\partial t} + A_0\left(E\frac{u}{L_0} + \frac{\mu}{L_0}\frac{du}{dt}\right) = F, \tag{A.7}$$

which is Eq. (9).

Proof of Theorem 1

Under the given conditions, the maturation, Ang-1 and Ang-2 equations can be rewritten as

$$\frac{dm}{dt} = b_m(1-m) - \mu_m m a_2 H(a_2 - \lambda a_1), \tag{A.8}$$

$$\frac{da_1}{dt} = b_{a_1} m + \mu_{a_1}(a_0 - a_1), \tag{A.9}$$

$$\frac{da_2}{dt} = b_{a_2}(1-m) - \mu_{a_2} a_2. \tag{A.10}$$

From (A.8), we obtain the inequality

$$\frac{dm}{dt} \le b_m(1-m), \tag{A.11}$$

which indicates that if the initial value of m is in $[0, 1]$, then it will remain in this range. Apparently, for any given m value, a_1 and a_2 will approach steady state values

$$a_1^* = \frac{b_{a_1} m}{\mu_{a_1}} + a_0, \tag{A.12}$$

$$a_2^* = \frac{b_{a_2}(1-m)}{\mu_{a_2}}. \tag{A.13}$$

Plugging these two values to (A.8) and assuming $\frac{dm}{dt} = 0$, we obtain

$$0 = b_m(1-m) - \mu_m m a_2^* H\left(a_2^* - \lambda a_1^*\right). \tag{A.14}$$

If $a_2^* < \lambda a_1^*$, then $m = 1$ from (A.14), as desired.
If $a_2^* > \lambda a_1^*$, then

$$0 = b_m(1-m) - \mu_m m\frac{b_{a_2}(1-m)}{\mu_{a_2}}. \tag{A.15}$$

There are two steady states from (A.15): $m = 1$, and $m = \frac{\frac{b_m}{\mu_m}}{\frac{b_{a_2}}{\mu_{a_2}}}$. But the second one is larger than one by the given conditions, which is a contradiction to the fact shown at the beginning of this proof.

Therefore, there is only one steady state: $m = 1, a_1 = a_0 + \frac{b_{a_1}}{\mu_{a_1}}, a_2 = 0$. Around this steady state, Eq. (A.8) reduces to

$$\frac{dm}{dt} = b_m(1 - m), \tag{A.16}$$

then it is easy to see that the linear system composed by (A.16), (A.9), and (A.10) is asymptotically stable. □

Proof of Theorem 2

Assume a cell of mass $e = 1$ and initial quiescent level m_0 is at position $\mathbf{x}$ and satisfies the autonomous system (19), (20), (21), (22), whose solutions depend uniquely and continuously on the initial conditions and VEGF values $c(\mathbf{x})$. If the initial quiescent level m_0 tends to 1, then the time required for m to reach 1 tends to 0, but the time for e to double tends to infinity. Thus, there exists a critical value $m_c(\mathbf{x}) \geq 0$ for m_0, such that m reaches 1 no later than e doubles. Let $m_c = \sup_{\mathbf{x}\in\bar{\Omega}} m_c(\mathbf{x})$. If $m_0 > m_c$, then all the cells will become quiescent before mass doubling; therefore, no cells will divide. □

References

Addison-Smith, B., McElwain, D.L.S., Maini, P.K., 2008. A simple mechanistic model of sprout spacing in tumour-associated angiogenesis. J. Theor. Biol. 250, 1–15.

Amano, S., Rohan, R., Kuroki, M., Tolentino, M., Adamis, A.P., 1998. Requirement for vascular endothelial growth factor in wound- and inflammation-related corneal neovascularization. Invest. Ophthalmol. Vis. Sci. 39(1), 18–22.

Anderson, A.R.A., Chaplain, M.A.J., 1998b. Continuous and discrete mathematical models of tumor-induced angiogenesis. Bull. Math. Biol. 60, 857–900.

Anderson, A.R.A., Chaplain, M.A.J., 1998a. A mathematical model for capillary network formation in the absence of endothelial cell proliferation. Appl. Math. Lett. 11, 109–114.

Arakelyan, L., Vainstein, V., Agur, Z., 2002. A computer algorithm describing the process of vessel formation and maturation, and its use for predicting the effects of anti-angiogenic and anti-maturation therapy on vascular tumor growth. Angiogenesis 5(3), 203–214.

Ashara, T., Chen, D., Takahashi, T., Fujikawa, K., Kearney, M., Magner, M., Yancopoulos, G.D., Isner, J.M., 1998. Tie-2 receptor ligands, angiopoietin-1 and angiopoietin-2, modulate VEGF-induced postnatal neovascularisation. Circ. Res. 83, 233–240.

Augustin, H.G., Young Koh, G., Thurston, G., Alitalo, K., 2009. Control of vascular morphogenesis and homeostasis through the angiopoietin-tie system. Nat. Rev. Mol. Cell Biol. 10(3), 165–177.

Ausprunk, D.H., Folkman, J., 1977. Migration and proliferation of endothelial cells in preformed and newly-formed blood vessels during tumor angiogenesis. Microvasc. Res. 14, 53–65.

Balding, D., McElwain, D.L.S., 1985. A mathematical model of tumor-induced capillary growth. J. Theor. Biol. 114, 53–73.

Bauer, A., Jackson, T., Jiang, Y., 2007. A cell-based model exhibiting branching and anastomosis during tumor-induced angiogenesis. Biophys. J. 92, 3105.

Beck, H., Acker, T., Wiessner, C., Allegrini, P.R., Plate, K.H., 2000. Expression of Angiopoietin-1, Angiopoietin-2, and Tie receptors after middle cerebral artery occlusion in the rat. Am. J. Pathol. 157, 1473–1483.

Benjamin, L.E., Golijanin, D., Itin, A., Pode, D., Keshet, E., 1999. Selective ablation of immature blood vessels in established human tumors follows vascular endothelial growth factor withdrawal. J. Clin. Invest. 103(2), 159–165.

Byrne, H.M., Chaplain, M.A.J., 1995. Mathematical models for tumour angiogenesis: Numerical simulations and nonlinear wave solutions. Bull. Math. Biol. 57, 461–486.

Byrne, H.M., Chaplain, M.A.J., 1996. Explicit solutions of a simplified model of capillary sprout growth during tumor angiogenesis. Appl. Math. Lett. 9, 69–74.
Chan-Ling, T., 1997. Glial, vascular and neuronal cytogenesis in whole-mounted cat retina. Microsc. Res. Tech. 36, 1–16.
Chaplain, M.A.J., 1996. Avascular growth, angiogenesis and vascular growth in solid tumours: The mathematical modelling of the stages of tumour development. Math. Comput. Model. 23(6), 47–87.
Cho, A., Mitchell, L., Koopmans, D., Langille, B.L., 1997. Effects of changes in blood flow rate on cell death and cell proliferation in carotid arteries of immature rabbits. Circ. Res. 81, 328–337.
Costa, K.D., Sim, A.J., Yin, F.C., 2006. Non-hertzian approach to analyzing mechanical properties of endothelial cells probed by atomic force microscopy. J. Biomech. Eng. 128(2), 176–184.
Cursiefen, C., Hofmann-Rummelt, C., Küchle, M., Schlötzer-Schrehardt, U., 2003. Pericyte recruitment in human corneal angiogenesis: an ultrastructural study with clinicopathological correlation. Br. J. Ophthalmol. 87, 101–106.
Davis, S., Aldrich, T.H., Jones, P.F., Acheson, A., Compton, D.L., Jain, V., Ryan, T.E., Bruno, J., Radziejewski, C., Maisonpierre, P.C., Yancopoulos, G.D., 1996. Isolation of angiopoietin-1, a ligand for the Tie2 receptor, by secretion-trap expression cloning. Cell 87(7), 1161–1169.
De Smet, F., Segura, I., De Bock, K., Hohensinner, P.J., Carmeliet, P., 2009. Mechanisms of vessel branching: Filopodia on endothelial tip cells lead the way. Arterioscler. Thromb. Vasc. Biol. 29(5), 639–649.
Fiedler, U., Scharpfenecker, M., Koidl, S., Hegen, A., Grunow, V., Schmidt, J.M., Kriz, W., Thurston, G., Augustin, H.G., 2004. The Tie-2 ligand Angiopoietin-2 is stored in and rapidly released upon stimulation from endothelial cell Weibel–Palade bodies. Blood 103(11), 4150–4156.
Fiedler, U., Reiss, Y., Scharpfenecker, M., Grunow, V., Koidl, S., Thurston, G., Gale, N.W., Augustin, H.G., 2006. Angiopoietin-2 sensitizes endothelial cells to tnf-α and has a crucial role in the induction of inflammation. Nat. Med. 12(2), 235–239.
Gerhardt, H., Golding, M., Fruttiger, M., Ruhrberg, C., Lundkvist, A., Abramsson, A., Jeltsch, M., Mitchell, C., Alitalo, K., Shima, D., Betsholtz, C., 2003. VEGF guides angiogenic sprouting utilizing endothelial tip cell filopodia. J. Cell Biol. 161, 1163–1177.
Gevertz, J.L., Torquato, S., 2006. Modeling the effects of vasculature evolution on early brain tumor growth. J. Theor. Biol. 243, 517–531.
Gracheva, M.E., Othmer, H.G., 2004. A continuum model of motility in ameboid cells. Bull. Math. Biol. 66, 167–193.
Griffioen, A.W., Molema, J., 2000. Angiogenesis: Potentials for pharmacologic intervention in the treatment of cancer, cardiovascular diseases, and chronic inflammation. Pharmacol. Rev. 52(2), 237–268.
Guido, S., Tranquillo, R.T., 1993. A methodology for the systematic and quantitative study of cell contact guidance in oriented collagen gels. J. Cell Sci. 105, 317–331.
Harrington, H.A., Maier, M., Naidoo, L., Whitaker, N., Kevrekidis, P.G., 2007. A hybrid model for tumor-induced angiogenesis in the cornea in the presence of inhibitors. Math. Comput. Model. 46, 513–524.
Holash, J., Wiegand, S.J., Yancopoulos, G.D., 1999. New model of tumor angiogenesis: dynamic balance between vessel regression and growth mediated by angiopoietins and VEGF. Oncogene 18, 5356–5362.
Horowitz, A., Simons, M., 2008. Branching morphogenesis. Circ. Res. 103(8), 784–795.
Jackson, T.L., Zheng, X., 2009. A continuous model of angiogenesis: initiation, extension and maturation modulated by vascular endothelial growth factor and angiopoietins (in preparation).
Jain, H.V., Nör, J.E., Jackson, T.L., 2008. Modeling the VEGF–Bcl-2–CXCL8 pathway in intratumoral angiogenesis. Bull. Math. Biol. 70, 89–117.
Karl, E., Warner, K., Zeitlin, B., Kaneko, T., Wurtzel, L., Jin, T., Chang, J., Wang, S., Wang, C., Strieter, R.M., Nunez, G., Polverini, P.J., Nor, J.E., 2005. Bcl-2 Acts in a Proangiogenic Signaling Pathway through Nuclear Factor-kappaB and CXC Chemokines. Cancer Res. 65(12), 5063–5069.
Kearney, J.B., Kappas, N.C., Ellerstrom, C., DiPaola, F.W., Bautch, V.L., 2004. The VEGF receptor (VEGFR1) is a positive modulator of vascular sprout formation and branching morphogenesis. Blood 103, 4527–4535.
Lamalice, L., Boeuf, F.L., Huot, J., 2007. Endothelial cell migration during angiogenesis. Circ. Res. 100, 782–794.
Larripa, K., Mogilner, A., 2006. Transport of a 1d viscoelastic actin-myosin strip of gel as a model of a crawling cell. Physica A 372, 113–123.
Levine, H.A., Nilsen-Hamilton, M., 2006. Angiogenesis-a biochemial/mathematical perspective. In: Friedman, A. (Ed.), Tutorials in Mathematical Biosciences III, Lecture Notes in Mathematics, vol. 1872, p. 65. Springer, Berlin, Chap. 2.

Levine, H.A., Pamuk, S., Sleeman, B.D., Nilsen-Hamilton, M., 2001a. Mathematical modeling of capillary formation and development in tumor angiogenesis: Penetration into the stroma. Bull. Math. Biol. 63, 801–863.

Levine, H.A., Sleeman, B.D., Nilsen-Hamilton, M., 2001b. Mathematical modeling of the onset of capillary formation initiating angiogenesis. J. Math. Biol. 42, 195–238.

Mac Gabhann, F., Popel, A.S., 2004. Model of competitive binding of vascular endothelial growth factor and placental growth factor to vegf receptors on endothelial cells. Am. J. Physiol. Heart Circ. Physiol. 286(1), H153–164.

Maisonpierre, P.C., Suri, C., Jones, P.F., Bartunkova, S., Wiegand, S.J., Radziejewski, C., Compton, D., McClain, J., Aldrich, T.H., Papadopoulos, N., Daly, T.J., Davis, S., Sato, T.N., Yancopoulos, G.D., 1997. Angiopoietin-2, a natural antagonist for Tie2 that disrupts in vivo angiogenesis. Science 277, 55–60.

Mantzaris, N., Webb, S., Othmer, H.G., 2004. Mathematical modeling of tumor-induced angiogenesis. J. Math. Biol. 49, 111–187.

Milde, F., Bergdorf, M., Koumoutsakos, P., 2008. A hybrid model for three-dimensional simulations of sprouting angiogenesis. Biophys. J. 95, 3146–3160.

Munevar, S., Wang, Y.-L., Dembo, M., 2001. Traction force microscopy of migrating normal and H-ras transformed 3T3 fibroblasts. Biophys. J. 80, 1744–1757.

Oliner, J., et al., 2004. Suppression of angiogenesis and tumor growth by selective inhibition of angiopoietin-2. Cancer Cell 6(5), 507–516.

Othmer, H., Stevens, A., 1997. Aggregation, blowup, and collapse: The ABC's of taxis in reinforced random walks. SIAM J. Appl. Math. 57, 1044–1081.

Paweletz, N., Knierim, M., 1989. Tumor related angiogenesis. Crit. Rev. Oncol. Hematol. 9, 197–242.

Peirce, S.M., Van Gieson, E.J., Skalak, T.C., 2004. Multicellular simulation predicts microvascular patterning and in silico tissue assembly. FASEB J., Feb. 2004.

Pettet, G.J., Byrne, H.M., McElwain, D.L.S., Norbury, J., 1996a. A model of wound-healing angiogenesis in soft tissue. Math. Biosci. 263, 1487–1493.

Pettet, G., Chaplain, M.A.J., McElwain, D.L.S., Byrne, H.M., 1996b. On the role of angiogenesis in wound healing. Proc. R. Soc. Lond. Ser. B 263, 1487–1493.

Plank, M.J., Sleeman, B.D., 2003. A reinforced random walk model of tumor angiogenesis and anti-angiogenesis strategies. IMA J. Math. Appl. Med. Biol. 20, 135–181.

Plank, M.J., Sleeman, B.D., 2004. Lattice and non-lattice models of tumour angiogenesis. Bull. Math. Biol. 66, 1785–1819.

Plank, M.J., Sleeman, B.D., Jones, P.F., 2004. A mathematical model of tumour angiogenesis, regulated by vascular endothelial growth factor and the angiopoietins. J. Theor. Biol. 229, 435–454.

Pollard, T.D., Borisy, G., 2003. Cellular motility driven by assembly and disassembly of actin filaments. Cell 112, 453–465.

Prass, M., Jacobson, K., Mogilner, A., Radmacher, M., 2006. Direct measurement of the lamellipodial protrusive force in a migrating cell. J. Cell Biol. 174(6), 767–772.

Purhonen, S., Palm, J., Rossi, D., Kaskenpää, N., Rajantie, I., Ylä-Herttuala, S., Alitalo, K., Weissman, I.L., Salven, P., 2008. Bone marrow-derived circulating endothelial precursors do not contribute to vascular endothelium and are not needed for tumor growth. PNAS 105, 6620–6625.

Qutub, A., Popel, A., 2009. Elongation, proliferation & migration differentiate endothelial cell phenotypes and determine capillary sprouting. BMC Syst. Biol. 3(1), 13.

Scharpfenecker, M., Fiedler, U., Reiss, Y., Augustin, H.G., 2005. The Tie-2 ligand Angiopoietin-2 destabilizes quiescent endothelium through an internal autocrine loop mechanism. J. Cell Sci. 118, 771–780.

Schugart, R.C., Friedman, A., Zhao, R., Sen, C.K., 2008. Wound angiogenesis as a function of tissue oxygen tension: A mathematical model. PNAS 105, 2628–2633.

Semino, C.E., Kamm, R.D., Lauffenburger, D.A., 2006. Autocrine EGF receptor activation mediates endothelial cell migration and vascular morphogenesis induced by VEGF under interstitial flow. Exp. Cell Res. 312, 289–298.

Serini, G., Ambrosi, D., Giraudo, E., Gamba, A., Preziosi, L., Bussolino, F., 2003. Modeling the early stages of vascular network assembly. EMBO 22, 1771–1779.

Sherratt, J.A., Murrat, J.D., 1990. Models of epidermal wound healing. Proc. R. Soc. Lond. B 241, 29–36.

Sholley, M.M., Wilson, J.D., 1987. Proliferation and migration of irradiated endothelial cells. In: Rifkin, D.B., Klagsbrun, M. (Eds.), Current Communications in Molecular Biology, pp. 139–144. Cold Spring Harbor Laboratory, Cold Spring Harbor.

Sholley, M.M., Wilson, J.D., Montour, J.L., 1983a. Effect of X-irradiation on proliferation of microvascular endothelial cells. Radiat. Res. 94, 648–649.

Sholley, M.M., Wilson, J.D., Montour, J.L., 1983b. Microvascular growth in X-irradiated rat corneas. Radiat. Res. 94, 649.

Sholley, M.M., Ferguson, G.P., Seibel, H.R., Montour, J.L., Wilson, J.D., 1984. Mechanisms of neovascularization. Vascular sprouting can occur without proliferation of endothelial cells. Lab. Invest. 51, 624–634.

Sleeman, B.D., Wallis, I.P., 2002. Tumour induced angiogenesis as a reinforced random walk: modeling capillary network formation without endothelial cell proliferation. J. Math. Comput. Model. 36, 339–358.

Stokes, C.L., Lauffenburger, D.A., 1991. Analysis of the roles of microvessel endothelial cell random mobility and chemotaxis in angiogenesis. J. Theor. Biol. 152, 377–403.

Sun, S., Wheeler, M.F., Obeyesekere, M., Patrick, C., 2005. A deterministic model of growth factor-induced angiogenesis. Bull. Math. Biol. 67, 313–337.

Sundberg, C., Kowanetz, M., Brown, L.F., Detmar, M., Dvorak, H.F., 2002. Stable expression of angiopoietin-1 and other markers by cultured pericytes: Phenotypic similarities to a subpopulation of cells in maturing vessels during later stages of angiogenesis in vivo. Lab. Invest. 82(4), 387–401.

Suri, C., Jones, P.F., Patan, S., Bartunkova, S., Maisonpierre, P.C., Davis, S., Sato, T.N., Yancopoulos, G.D., 1996. Requisite role of angiopoietin-1, a ligand for the tie2 receptor, during embryonic angiogenesis. Cell 87(7), 1171–1180.

Szabo, A., Perryn, E.D., Czirok, A., 2007. Network formation of tissue cells via preferential attraction to elongated structures. Phys. Rev. Lett. 98, 038102.

Thompson, L.J., Wang, F., Proia, A.D., Peters, K.G., Jarrold, B., Greis, K.D., 2003. Proteome analysis of the rat cornea during angiogenesis. Proteomics 3, 2258–2266.

Thoumine, O., Ott, A., 1997. Time scale dependent viscoelastic and contractile regimes in fibroblasts probed by microplate manipulation. J. Cell Sci. 110, 2109–2116.

Tong, S., Yuan, F., 2001. Numerical simulations of angiogenesis in the cornea. Microvasc. Res. 61, 14–27.

Tong, S., Yuan, F., 2008. Dose response of angiogenesis to basic fibroblast growth factor in rat corneal pocket assay: II. Numerical simulations. Microvasc. Res. 75, 16–24.

Wakui, S., Yokoo, K., Muto, T., Suzuki, Y., Takahashi, H., Furusato, M., Hano, H., Endou, H., Kanai, Y., 2006. Localization of Ang-1, -2, Tie-2, and VEGF expression at endothelial-pericyte interdigitation in rat angiogenesis. Lab. Invest. 86, 1172–1184.

Wang, D., Lehman, R.E., Donner, D.B., Matli, M.R., Warren, R.S., Welton, M.L., 2002. Expression and endocytosis of VEGF and its receptors in human colonic vascular endothelial cells. Am. J. Physiol. Gastrointest. Liver Physiol. 282(6), G1088–1096.

White, R.R., Shan, S., Rusconi, C.P., Shetty, G., Dewhirst, M.W., Kontos, C.D., Sullenger, B.A., 2003. Inhibition of rat corneal angiogenesis by a nuclease-resistant rna aptamer specific for angiopoietin-2. PNAS 100(9), 5028–5033.

Witzenbichler, B., Maisonpierre, P.C., Jones, P., Yancopoulos, G.D., Isner, J.M., 1998. Chemotactic properties of angiopoietin-1 and -2, ligands for the endothelial-specific receptor tyrosine kinase Tie-2. J. Biol. Chem. 273, 18514–18521.

Zeng, G., Taylor, S.M., McColm, J.R., Kappas, N.C., Kearney, J.B., Williams, L.H., Hartnett, M.E., Bautch, V.L., 2007. Orientation of endothelial cell division is regulated by VEGF signaling during blood vessel formation. Blood 109(4), 1345–1352.